ELSEVIER

Contents lists available at ScienceDirect

Biomaterials

journal homepage: www.elsevier.com/locate/biomaterials



In situ heart valve tissue engineering using a bioresorbable elastomeric implant — From material design to 12 months follow-up in sheep



Jolanda Kluin ^{a, b}, Hanna Talacua ^{a, b}, Anthal I.P.M. Smits ^{c, d}, Maximilian Y. Emmert ^{e, f, g}, Marieke C.P. Brugmans ^h, Emanuela S. Fioretta ^e, Petra E. Dijkman ^e, Serge H.M. Söntjens ⁱ, Renée Duijvelshoff ^{c, d}, Sylvia Dekker ^c, Marloes W.J.T. Janssen-van den Broek ^c, Valentina Lintas ^e, Aryan Vink ^j, Simon P. Hoerstrup ^{c, e, g}, Henk M. Janssen ⁱ, Patricia Y.W. Dankers ^{c, d}, Frank P.T. Baaijens ^{c, d}, Carlijn V.C. Bouten ^{c, d, *}

- ^a Department of Cardiothoracic Surgery, Academic Medical Center, Amsterdam, The Netherlands
- ^b Department of Cardiothoracic Surgery, University Medical Center, Utrecht, The Netherlands
- ^c Department of Biomedical Engineering, Eindhoven University of Technology, The Netherlands
- ^d Institute for Complex Molecular Systems (ICMS), Eindhoven University of Technology, The Netherlands
- e Institute for Regenerative Medicine (IREM), University of Zürich, Switzerland
- f Heart Center Zürich, University Hospital Zürich, Switzerland
- ^g Wyss Translational Center Zürich, ETH and University of Zürich, Switzerland
- ^h Xeltis BV, Eindhoven, The Netherlands
- ⁱ SyMO-Chem BV, Eindhoven, The Netherlands
- j Department of Pathology, University Medical Center, Utrecht, The Netherlands

ARTICLE INFO

Article history:
Received 7 September 2016
Received in revised form
21 December 2016
Accepted 6 February 2017
Available online 8 February 2017

Keywords:

Cardiovascular tissue engineering Endogenous regeneration Supramolecular chemistry Biodegradable polymers Pulmonary valve replacement Regenerative biomaterials

ABSTRACT

The creation of a living heart valve is a much-wanted alternative for current valve prostheses that suffer from limited durability and thromboembolic complications. Current strategies to create such valves, however, require the use of cells for *in vitro* culture, or decellularized human- or animal-derived donor tissue for *in situ* engineering. Here, we propose and demonstrate proof-of-concept of *in situ* heart valve tissue engineering using a synthetic approach, in which a cell-free, slow degrading elastomeric valvular implant is populated by endogenous cells to form new valvular tissue inside the heart. We designed a fibrous valvular scaffold, fabricated from a novel supramolecular elastomer, that enables endogenous cells to enter and produce matrix. Orthotopic implantations as pulmonary valve in sheep demonstrated sustained functionality up to 12 months, while the implant was gradually replaced by a layered collagen and elastic matrix in pace with cell-driven polymer resorption. Our results offer new perspectives for endogenous heart valve replacement starting from a readily-available synthetic graft that is compatible with surgical and transcatheter implantation procedures.

© 2017 The Authors. Published by Elsevier Ltd. This is an open access article under the CC BY-NC-ND license (http://creativecommons.org/licenses/by-nc-nd/4.0/).

1. Introduction

Current heart valve prostheses have serious drawbacks, such as thromboembolic complications or calcification-induced limited durability [1–3]. Most importantly, current prosthetic valves,

E-mail address: c.v.c.bouten@tue.nl (C.V.C. Bouten).

including cryopreserved donor valves, are non-living structures that do not adapt to functional demand changes, which inherently limits their durability in comparison to a viable valve replacement (i.e. a pulmonary homograft) [4]. As a result, pediatric patients in particular are faced with a lifelong risk of valve-related morbidity and up to 50% reduction in life expectancy [5]. The creation of living, tissue engineered heart valves that can last a lifetime is believed to overcome these limitations [6,7]. Classical heart valve tissue engineering (TE) in which cells are harvested, expanded *in vitro*, seeded on a rapidly-degrading scaffold and conditioned in a

^{*} Corresponding author. Eindhoven University of Technology, Dept. of Biomedical Engineering, Groene Loper 15 (GEM-Z 4.117), P.O. Box 513, 5600 MB, Eindhoven, The Netherlands.

bioreactor for several weeks to ensure fast matrix production that can withstand hemodynamic forces, has been explored for over 20 years [8—13]. Yet, translation to the clinic has proven difficult. This is mainly due to the complexity of the procedure and suboptimal long-term *in vivo* performance — the prevalent issue being valve leaflet retraction by the seeded cells [11—13]. To reduce these drawbacks, *in situ* heart valve TE has emerged to create living valves at the site of destination inside the heart. In this approach, a malfunctioning valve is replaced by a cell-free scaffold that gradually transforms into a living valve by recruiting endogenous cells and using the body as a "bioreactor".

Recent studies employing the in situ heart valve TE principle have shown compelling results using decellularized biological scaffolds, such as small intestine submucosa (SIS) [14,15] or de novo engineered extracellular matrices [13,16–18]. Moreover, promising results have been achieved using decellularized allografts, which have led to the large-scale clinical trials of these valves over the last decade [19–21]. However, these approaches do not negate the need for a (engineered) biological starter matrix and offer limited control over scaffold properties. Here we propose and demonstrate proof of concept of *in situ* heart valve TE starting from a cell-free synthetic bioresorbable micro-porous scaffold as a novel concept in heart valve replacement therapy (Fig. 1A). Compared to other (in situ) tissue engineering approaches, this fully synthetic approach is advantageous in that it does not require the use of any donor, using either human donor valves (decellularized allografts) or animalderived tissue (e.g. SIS), or even in vitro cell and tissue culture. The use of a synthetic starter matrix offers off-the-shelf availability at substantially reduced costs and logistic complexity by omitting any tissue culture or tissue preparation [22,23]. In addition, synthetic materials offer high control over scaffold design and manufacturing, including the modulation of scaffold properties (e.g. resorption rate, biophysical properties) to induce functional, healthy regeneration [24,25]. Last, but not least, regulatory complexity is drastically reduced because the synthetic scaffolds can be considered as medical device at the time of implantation. While this concept has been demonstrated for tissue engineered vascular grafts [26–28], synthetic material-based in situ heart valve TE poses more complex challenges related to the valvular geometry and the complex dynamic opening and closing of the valve. The scaffold should not only withstand hemodynamic loading immediately upon implantation, but also maintain stable valve function with time and during scaffold resorption and neo-tissue formation. To our opinion, safe clinical use requires that scaffold resorption should be mainly cell driven, meaning that the scaffold will only degrade, and thus lose strength and durability, when sufficient extracellular matrix has been synthesized by the cells to take over mechanical functionality.

The goal of the present study was to design a bioresorbable synthetic heart valve that can maintain long-term functionality as a pulmonary valve in sheep, recruit host cells, and support the *in situ* formation of neo-tissue by these cells in pace with scaffold resorption. Valve structural and mechanical properties, opening and closing behavior, and resorption mechanisms were tested *in vitro*, while long-term functionality and *in situ* cell recruitment and neo valve formation were studied during long-term follow-up in an ovine model.

2. Materials & methods

2.1. Valve design and in vitro testing

For the development of the valvular scaffold we considered the relevant design criteria over multiple length-scales. At the molecular level, we employed a custom-developed bioresorbable

supramolecular elastomer, based on bis-urea-modified polycarbonate (PC-BU). Using electrospinning, this material was processed into microporous scaffolds with fiber diameters and pore sizes optimized to advocate homogenous cell colonization and regenerative remodeling of the scaffold [28–30]. To characterize the mechanisms of scaffold resorption, scaffolds were subjected to accelerated hydrolysis and oxidative *in vitro* resorption tests. On the macroscopic scale, we developed a crown-shaped polyether ether ketone (PEEK) reinforcement ring to stabilize valve geometry. Prior to implantation, the polymer was seeded with fast-degrading fibrin gel in analogy with our previous *in vitro* heart valve TE approaches [31,32]. *In vitro* function of the resulting valvular device was tested in accordance with ISO 5840 using a pulsatile test system.

2.1.1. PC-BU polymer synthesis and characterization

PC-BU was developed and synthesized in-house in an analogous fashion to the preparation of the polycaprolactone bis-urea biomaterial as reported by Wisse et al. [33,34], by replacing the amine functional polycaprolactone used by Wisse et al. with amine functional polycarbonate in the chain extension polymerization reaction with butylene diisocyanate. The PC-BU material was analyzed by attenuated total reflectance Fourier transformed infrared (ATR-FTIR) spectroscopy as measured on a Spectrum Two IR spectrometer (Perkin Elmer). The neat PC-BU material was thermally analyzed by differential scanning calorimetry (DSC) using a Q2000 machine (TA Instruments). Melting (T_m) and glass (T_g) transition temperatures were measured from the melt, i.e. after the sample had first been brought to the isotropic state, in the second or ensuing heating runs. Heating scan rates of 10 °C/min and 40 °C/ min were used for T_m and T_g assessment, respectively. The T_m was determined by the peak temperature, while the Tg was given by the inflection point in the thermogram. The degradative properties of PC-BU were assessed using accelerated in vitro tests, as previously described [35] (Supplementary Dataset 1).

2.1.2. Cytotoxicity test

A PC-BU solvent-cast film was prepared using chloroform/ methanol as solvent, and was dried under vacuum to remove traces of solvent. Film samples were incubated in complete culture medium (DMEM from Gibco, supplemented with 10% (v/v) fetal bovine serum (FBS) and 1% (v/v) Penicillin Streptavidin) at 37 °C and 5% CO₂. Extraction of the PC-BU samples was performed for 24 h at a weight per volume of 20 mg PC-BU per mL complete medium. 3T3 mouse fibroblasts were seeded at a density a 5×10^3 cells per well in a 96-well plate and were maintained for 24 h under standard culturing conditions until cells were grown to 50% confluence. Next, the medium was removed and the 3T3 fibroblasts were cultured for an additional 24 h in the presence of 100 µL of filtered medium extract (n = 4). Cells exposed to complete medium supplemented with 1% (v/v) Triton-X 100 served as a control for cytotoxic conditions. The cytotoxicity was determined using an MTT cytotoxicity assay. Briefly, thiazolyl blue tetrazolium bromide (MTT, from Sigma) was dissolved in phosphate buffered saline to a concentration of 5 mg/mL; the solution was filtered and further diluted in complete medium to a final concentration of 1 mg/mL. The extract medium was removed and replaced with 50 µL of the MTT/culture medium. Fibroblasts were incubated for 2 h under standard culturing conditions, before the MTT solution was removed and replaced with 100 µL of isopropanol (acidified with 0.04 M HCl) until all formazan crystals dissolved. Subsequently, the absorbance was measured at 570 nm (650 nm reference wavelength) on a Tecan Safire microplate reader. Cell viability is presented relative to that of 3T3 fibroblasts that were maintained in untreated culture medium during the course of the study, where this reference is set at 100% cell viability.

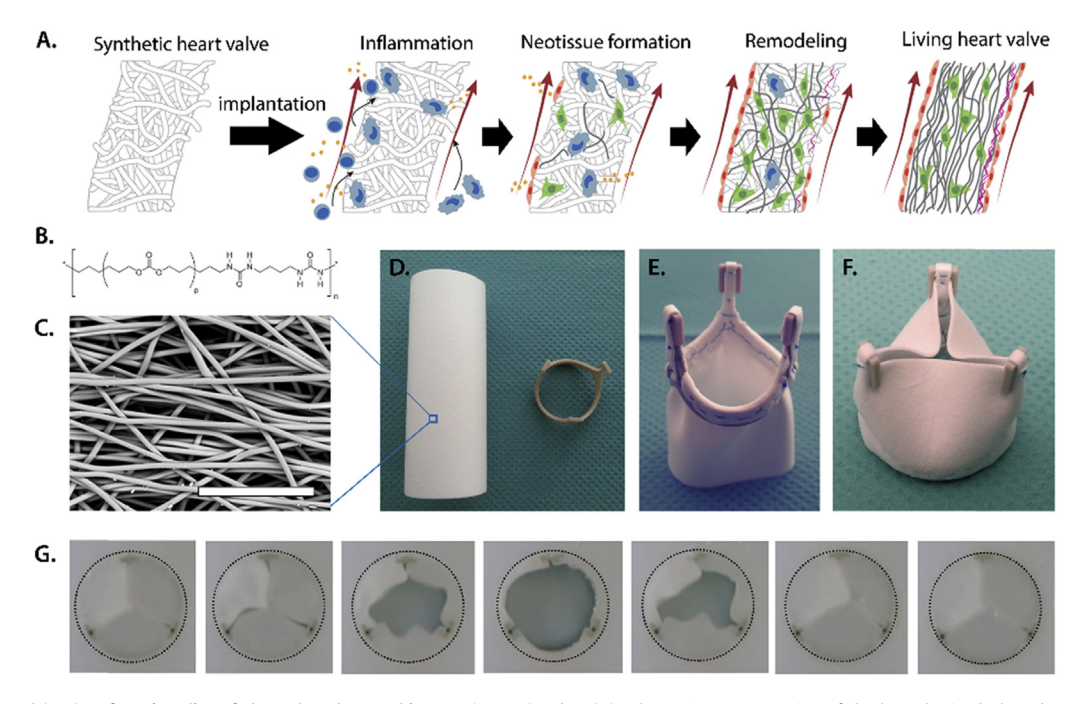


Fig. 1. Fabrication and *in vitro* functionality of the polycarbonate bis-urea (PC-BU) valve. (A) Schematic representation of the hypothesized phased process of regeneration, mirroring the wound healing cascade, moving form an acellular synthetic graft into an autologous living valve. (B) The strictly segmented sequence controlled molecular structure of PC-BU (p is on average approximately 16–17). (C) Scanning electron microscopy image of the fibrous microstructure of the valve. Scale bar, 50 μm. (D–F) The valve is composed of an electrospun PC-BU tube sutured onto a reinforcement crown. (G) Movie stills of an *in vitro* valve functionality test demonstrating good closure and opening behavior, in accordance with ISO 5840 criteria.

2.1.3. Uniaxial tensile testing

The bulk mechanical properties of the PC-BU base material were determined by performing uniaxial stress-strain tensile tests on dog-bone shaped solid samples (length =22 mm, width =5 mm, thickness $=0.30\,\pm\,0.04$ mm) as prepared and punched from chloroform/methanol (v/v 3:1) solution cast films. The tensile tests were executed at room temperature, using a crosshead speed of 20 mm/min. Measured stresses (σ) and strains (ϵ) were engineering stresses and strains. Reported values represent the average \pm standard deviation (n =3).

2.1.4. Electrospinning

The valves were manufactured by suturing an electrospun tube of PC-BU on a polyether ether ketone (PEEK) supporting stent. For electrospinning, the PC-BU polymer was dissolved in solvents and stirred overnight. Following complete dissolution, the polymers were electrospun in a climate-controlled electrospinning apparatus (IME Technologies). The polymer solution was delivered at a constant flow rate to a metal capillary connected to a high-voltage power supply. A grounded rotating mandrel was used as a collector. As the polymer jet accelerated towards the collector, the solvent evaporated and a charged polymer fiber was deposited on the rotating target in the form of a non-woven mesh. Fiber morphology and diameter were evaluated by scanning electron microscopy (SEM) (Phenom World Phenom Pro, Fibermetric® software). Scaffold thickness was measured with a digital thickness gauge (Mitutoyo SGM).

2.1.5. Support ring

The design of the reinforcement ring was generated using computer-aided design software (Autodesk Inventor). The crownlike structure of the support consisted of a ring with three individual posts and measured 20 mm in outer diameter. The ring connecting the three posts contained small holes (\varnothing 0.8 mm) for

suturing. Supports were made out of a solid piece of PEEK by using computer controlled milling technology. Valves were fabricated by suturing the electrospun PC-BU tubes onto the support ring by using 6-0 prolene sutures (Ethicon, Johnson & Johnson Medical). Valves were sterilized by Ethylene Oxide sterilization (Synergy Health).

2.1.6. Fibrin coating

Prior to implantation, valves were coated with fibrin. Valves were placed in 70% ethanol (VWR) for 1 min, washed three times with phosphate buffered saline (PBS; Sigma), and placed in culture medium overnight, consisting of advanced Dulbecco's Modified Eagle Medium (DMEM; Gibco), supplemented with 10% lamb serum (Gibco), 1% L-Glutamine (Lonza), and 1% penicillin/streptomycin (Lonza), further referred to as standard medium. Prior to fibrin coating, the medium was aspirated from the scaffold. For fibrin gel formation, sterile bovine fibrinogen solution, with 10 mg actual protein/mL medium (Sigma), was added to sterile bovine thrombin solution, with a concentration of 10 IU thrombin/mL medium (Sigma). A total volume of 100 µL fibrin per 100 mm³ scaffold was used. Coated valves were placed in an incubator for 15 min to allow for fibrin polymerization, followed by the addition of standard medium. Coated valves were stored at 37 °C until implantation.

2.1.7. Hydrodynamic in vitro functionality assessment

One valve was used for *in vitro* valve functionality assessment. The valve was placed inside a silicon annulus of 21 mm inner diameter and positioned into a hydrodynamic pulsatile test system (HDT-500, BDC laboratories) containing a physiologic saline solution at 37 °C. The valve was subjected to physiological pulmonary conditions (rate of 72 beats per minute, stroke volume of 70 mL, maximum diastolic pressure difference of 25 mmHg) for 1 h. Flow and pressures were measured via an ultrasonic flow module

(TS410, Transonic Systems) and pressure sensors (BDC-TP, BDC Laboratories), respectively. Data was collected for 5 s at 5 kHz and functionality was assessed from an average over 10 cardiac cycles by using Statys $^{\text{TM}}$ software (BDC Laboratories) to determine cardiac output (CO), effective orifice area (A_{EO}) and regurgitation fraction (RF), as well as stroke, leakage and closing volume. Slow-motion movies were recorded to assess opening and closure behavior of the valve, as well as leaflet motion (G15 Powershot, Canon).

After pulsatile functionality assessment, the silicon annulus containing the valve was positioned into a valve durability tester (VDT-3600i, BDC Laboratories) containing a physiologic saline solution at 37 °C. The valve was subjected to pulmonary conditions for one million cycles, before it was subjected to aortic conditions until failure. Slow-motion movies were recorded to assess opening and closure behavior of the valve, as well as leaflet motion (G15 Powershot, Canon).

2.2. Sheep studies

In vivo functionality as pulmonary valve replacement was studied during long-term follow-up in an ovine model. Following a successful *in vivo* pilot of 2 months follow-up (n=1), we monitored valve function, *in situ* cell recruitment, neo-tissue formation, *in vivo* scaffold resorption and mechanical properties of valves up to 6 (n=5) and 12 (n=4) months follow-up.

2.2.1. Animals

Approval for the animal studies was obtained by the University Medical Center Utrecht Animal Care Ethics committee and are in agreement with the current Dutch law on animal experiments. Ten female swifter sheep (mean weight 67.8 kg, mean age 2.8 years) underwent pulmonary valve replacement. Follow-up was 2 months (n=1), 6 months (n=5), and 12 months (n=4).

2.2.2. Anesthesia

Buprenorphine (5 mcg/hr patch; Bu Trans, Mundipharma DC) and Diazepam (10 mg orally; Diazepam CF, Centrafarm) was given as pre-medication, one day prior to pulmonary valve replacement. On the day of surgery, ketamin/hydrochlorin (10 mg/kg IM; Narketan 10, Vétoquinol) and Midazolam (0,4 mg/kg IM; Midazolam Actavis 5 mg/ml, Actavis) was given as a pre-anesthetic. Propofol was used as induction anesthesia (2-4 mg/kg; Propofol 20 mg/ml, Fresenius Kabi) and Propofol (4-7 mg/kg; Propofol 20 mg/ml, Fresenius Kabi) and Sufenta forte (5 µg/kg; Sufentanil-Hameln, 50 mcg/ml, Hameln) was given to maintain anesthesia during surgery. Furthermore, prophylactic Amiodarone (150 mg; Cordarone 50 mg/ml, Sanofi-Aventis) was given intravenously to prevent arrhythmias. Furosemide (2 dd 20 mg; Furosemide 20 PHC, Pharmachemie BV) and Flunixinemeglumine (1 dd 0.02 ml/kg; Cronyxin, 50 mg/ml, Dechra) was given during the first three days post-operatively. Animals received life-long Ascal (1 dd 80 mg orally; Ratiopharm).

2.2.3. Pulmonary valve replacement

During surgery animals were monitored in terms of ECG, arterial blood pressure, capnography, and temperature. Animals were placed in the right lateral position. Heparin was administered intravenously. Animals were placed on cardiopulmonary bypass. For arterial access, an 18 Fr arterial cannula (Edwards Lifescienes) was placed in the left arotid artery. A 27 Fr venous cannula (Biomedics) was placed in the left jugular vein. A left-sided anterolateral thoracotomy was performed in the third or fourth intercostal space. The pericardium was opened and a length incision in the pulmonary artery was made distally from the native pulmonary valve. The cusps of the native pulmonary valve were

excised. The cell-free biodegradable heart valve device was implanted using continuous sutures (5-0 Prolene C1). After careful de-airing, the pulmonary artery was closed in a continuous fashion (5-0 Prolene C1). After weaning from extracorporeal circulation, an epicardial echocardiography using a Philips iE33 echocardiography machine was made to assess valve function. Protamine was administered intravenously and the cannulas were removed. A chest tube was placed in the left thoracic cavity and the wound was closed in layers.

2.2.4. In vivo valve function and explantation

Anesthetic protocol during explantation was similar to implantation. A mid-sternotomie was performed and afterwards an epicardial echocardiography using a Philips iE33 echocardiography machine was performed to assess in vivo valve performance. The pulmonary valve area (PVA) was determined from the echocardiography and valve insufficiency was graded (grade 1: jet < 25%, vena contracta < 3 mm; grade 3: jet 25-65%, vena contracta 3-6 mm). Additionally, invasive pressure measurements were conducted in the right ventricle outflow tract and pulmonary artery. Thereafter, the heart, liver, spleen and lungs were explanted and the animals exsanguinated. The implanted valves were explanted from the heart. After macroscopic inspection of the organs and the explanted valve prosthesis, the valve was carefully freed from the PEEK reinforcement ring. The valve was transected in longitudinal direction to expose the leaflets. The average leaflet length was approximated from macroscopic images by measuring the distance from the hinge point to the free edge at the center of the leaflets for all three leaflets and averaged per valve. Reported data is the average of all valves per time point \pm standard deviation. The peripheral organs were transected and the valve leaflets were transected following a standard cutting protocol (Fig. S1).

2.3. Explant evaluation

2.3.1. Histology

Prior to embedding in paraffin, samples were fixated in 10% formalin and embedded in agar gel to prevent damage to the polymeric fibers during the paraffin-embedding protocol. Peripheral organs were embedded without agar. Stainings were performed on longitudinal 4 µm serial sections after deparaffinization in xylene and rehydration in a graded series of ethanol. Sections were stained with Weigert's Hematoxylin and Eosin (H&E) to assess gross morphology, Masson's Trichrome (Sigma-Aldrich) to assess extracellular matrix, Rusell-Movat Pentachrome (American MasterTech) to assess tissue composition, Picrosirius Red (Sirius red F3B, Sigma, in saturated aqueous picric acid, Fluka) to assess collagen, and Alizarin Red (Sigma) to assess calcium deposits. The leaflet thickness was measured in the microscopic images in three locations per leaflet (i.e. hinge, belly and free edge). Reported data is the average per location of all valves per timepoint ± standard deviation.

2.3.2. Immunohistochemistry

Following deparaffinization, antigen retrieval was performed in a 96 °C water bath for 20 min in a modified citrate buffer (pH 6.1; DAKO). Enzymatic antigen retrieval (for Elastin, Fibrillin-1 and Fibrillin-2 antibodies) was performed with pepsin (0.05% in 10 mM HCl; Sigma) for 12 min at 37 °C. Depending on the antibody used this was followed by a permeabilization step with 0.5% Triton-X100 (Merck) in PBS (Sigma). Blocking was performed by incubating slides in 1% non-fat dry milk, 1% BSA and 2% normal goat serum (Invitrogen) at room temperature for 2 h. Primary antibodies (Table 1) were prepared at the desired concentrations in 1:10 diluted blocking buffer and were applied overnight at 4 °C. All

washing steps were done with 0.05% Tween-20 (Merck) in PBS or 0.05% Tween-20 in TBS.

Alkaline phosphatase-labeled (AP; Abcam) secondary antibodies were used in a 1:500 dilution. AP activity was visualized with SIGMA FAST™ BCIP/NBT (5-Bromo-4-chloro-3-indolyl phosphate/Nitro blue tetrazolium; pH 9.5, Sigma). Counterstaining was performed with Nuclear Fast Red (Sigma). For immunofluorescence, Alexa 488/555/647 or Strepavidin-Alexa 555 for biotinylated primary antibodies were used as the labels. Cell nuclei were stained with 4′,6-diamidino-2-phenylindole (DAPI). Incubations with the secondary antibody only were included as negative controls. Stained slides were dehydrated and mounted in Entellan (Merck) or Mowiol (Calbiochem). Tile scans and pictures were recorded with a Zeiss Axio Observer Z1 microscope or a Zeiss Axiovert fluorescence microscope using Zeiss ZEN software.

Histological quantification was performed on high-power magnification images ($40\times$ objective, Nikon E800 microscope with ACT-1 software) by two investigators who were blinded to follow-up time and number of the animal. A total of 7 areas, in the center of the scaffold, over the total length of the leaflet were analyzed, from the base to the tip of the leaflet (Fig. 3B). To quantify α -smooth muscle actin (α -SMA) expression per area, images were binarised and the area of positive signal was determined per high-power field (hpf). To compare the α -SMA expression between 6 and 12 months, the values from each region were summed per valve and averaged per time point.

2.3.3. Biochemical analysis

The tissue composition of explants was quantified in terms of DNA, glycosaminoglycan (GAG), hydroxyproline (HYP), and elastin. For this, samples were incubated overnight at 60 °C in a digestion buffer with papain (Sigma). After digestion, the GAG content was measured using a modification of the assay as previously described by Farndale et al. [36], with shark chondroitin sulfate (Sigma) as a reference. The total amount of DNA in the samples was quantified using the Hoechst dye method [37] with a reference curve prepared from calf thymus DNA (Sigma). The hydroxyproline (HYP) quantity was determined as a measure of collagen content, following the methods described by Huszar et al. [38] with *trans*-4-hydroxyproline (Sigma) as the reference. Elastin content was determined using the Fastin Elastin assay (Biocolor) according to the manufacturer's protocol.

2.3.4. Scanning electron microscopy (SEM)

Samples were analyzed by SEM to visualize coverage of the scaffold with neo-tissue and to visualize the degree of degradation of scaffold fibers. To assess neo-tissue coverage and endothelialization of the implanted scaffolds, samples were fixed in glutaral-dehyde and dehydrated in a graded ethanol series, starting from 50% to 100% in 5–20% increments. The ethanol was then allowed to evaporate, and samples were gold-sputtered for visualization. To visualize morphology and degree of degradation of the scaffold

fibers, neo-tissue was removed by incubation of the explant with 4.6% sodium hypochlorite (clorox) for 15 min at room temperature and washing twice in purified water. The samples, either glutaraldehyde-fixed or clorox-treated, were analyzed by SEM (Quanta 600F, FEI).

2.3.5. Gel Permeation Chromatography (GPC)

For every explant material sample, two separate sample solutions were prepared by dissolving explant sample in eluent, constituted of dimethylformamide with 0.25% (v/v) water and 0.1% (w/w) lithium bromide. A concentration of approximately 1 mg material per mL of eluent was used. Prior to measurement, the sample solutions were filtered over 0.2 μm filters to remove minor insolubles. A Varian/Polymer Laboratories PL-GPC 50 operated at 50 °C equipped with a Shodex GPC KD-804 column was used to determine number averaged molecular weights $(M_{\rm m})$ and weight averaged molecular weights $(M_{\rm w})$. The measured data are relative to polyethylene glycol (PEG) standards.

2.3.6. Biaxial tensile tests

Mechanical properties of a non-implanted control scaffold, the explants, and native control valves were analyzed by using a biaxial tensile tester (BioTester, 1.5 N load cell; CellScale) in combination with LabJoy software (V8.01, CellScale). Two square samples $(6 \times 6 \text{ mm}^2)$ per valve were symmetrically cut from the belly region. Sample thickness was measured at 3 random locations using an electronic caliper (CD-15CPX, Mitutoyo) and averaged. The samples were stretched equibiaxially in the radial and circumferential direction up to 30% strain, at a strain rate of 100% per minute. After stretching, the samples recovered to 0% strain at a strain rate of 100% per minute, followed by a rest cycle of 54 s. Prior to measuring the final stresses, samples were preconditioned with 5 of these cycles. A high-order polynomial curve was fitted through each individual data set in both the radial and circumferential direction. Two of the 12-month explants could not be analyzed due to technical failure during testing.

2.3.7. Statistical analysis

Given the limited sample size, the data could not be tested for Gaussian distribution. Therefore, we used non-parametric tests for statistical analysis. To compare the average values for DNA, GAG and HYP between the 6- and 12-months explants and the native pulmonary valve, the data was tested using a Kruskal-Wallis test with Dunn's Multiple Comparison post-hoc test (n = 5 for 6 months, n = 4 for 12 months and native). For the elastin content, and the leaflet length and thickness measurements, the native pulmonary valve (with n = 1) was not included in statistical analysis and the 6- and 12-months explants were compared via Mann-Whitney test.

Table 1 Primary antibodies used for immunohistochemical analysis.

Antibody	Host	Isotype	Supplier	Catalog number	Antigen retrieval	Dilution
Vimentin	Mouse	IgM	Abcam	Ab20346	Citrate	1:1200
α-SMA	Rabbit	IgG	Abcam	Ab5694	Citrate	1:600
CD31	Mouse	IgG2a	Novus Biologicals	NB100-65900	Citrate	1:100
Elastin	Mouse	IgG1	Abcam	Ab9519	Pepsin	1:200
Collagen I	Rabbit	IgG	Abcam	Ab34710	Citrate	1:200
Fibrillin-1-bio	Rabbit	IgG	Sigma	HPA017759	Pepsin	1:200
Fibrillin-2	Rabbit	IgG	Sigma	HPA012853	Pepsin	1:200
CD45	Mouse	IgG1	AbD Serotec	MCA2220GA	None	1:400

3. Results

3.1. From biomaterial to a functional valvular device

The synthesized PC-BU biomaterial has a novel molecular structure with uniform and strictly segmented poly-n-hexylcarbonate soft blocks and butylene bis-urea hard blocks (Fig. 1B). The polycarbonate soft block has a number average molecular weight of approximately 2.5 kDa and alternates with the hard block. Every hard block along the polymer chain is the same and is a butylene bis-urea group. Accordingly, PC-BU has a sequence-controlled macromolecular structure. ATR-FTIR analysis revealed a major resonance at 1741 cm⁻¹ for the carbonate groups in PC-BU, and further resonances at 3326, 1619 and 1577 cm^{-1} for the urea groups (Fig. S2). These three wavelength positions are indicative of strongly hydrogen bonded ureas [39]. Differential scanning calorimetry analyses confirmed the expected phase-separated morphology that is typical for thermoplastic elastomers, with a 'soft' amorphous phase (a T_g at $-40~^{\circ}\text{C}$ and a T_m at ca. 5 $^{\circ}\text{C})$ and a 'hard' crystalline phase (T_m at ca. 138 °C) due to the strongly hydrogen-bonded bis-urea groups (Fig. S2). PC-BU is not cytotoxic, as determined by MTT assay (Fig. S2).

Tensile testing of the bulk PC-BU showed a stress-strain curve with a monotonous increase of stress, without displaying a distinct yield point (σ_{yield}) . Therefore, the strength at break (σ_{break}) was also the ultimate tensile strength (UTS), which was determined to be 39.8 \pm 1.6 MPa at a maximum strain at break (ϵ_{break}) of 952 \pm 21%. The tensile toughness (or UT; as determined by the area under the stress-strain curve) was determined to be 190 \pm 9 MPa, with a Young's modulus (E; as determined between 0.25% and 2.5% strain) of 11.2 \pm 0.2 MPa.

The material was processed using electrospinning and resulting meshes were characterized with SEM (Fig. 1C). The fiber diameter and pore size (fiber \varnothing 4.04 \pm 0.25 μm ; porosity 78–81%) were optimized to enable circulating and tissue cells to enter the scaffold. Accelerated in vitro degradation tests showed that electrospun PC-BU meshes are prone to both hydrolysis and oxidation, although PC-BU is less affected by oxidative degradation when compared to polyester-based supramolecular materials [35] (Supplemental Dataset 1).

Valves were manufactured by shaping and suturing electrospun PC-BU tubes onto a crown-shaped PEEK reinforcement ring (Fig. 1D—F). Function of the resulting valvular device was tested in accordance with ISO 5840; *in vitro* using a pulsatile test system under elevated pulmonary pressures (50/25 mmHg) and aortic pressures (120/80 mmHg) at a cardiac output of 5 L/min and heart rate of 70 bpm for 20 h. The valve showed good opening and closure behavior (Fig. 1G and Supplementary Movie 1). Cardiac output, effective orifice area, and regurgitation fraction met ISO 5840 criteria for cardiac valve prostheses (5.34 L/min, 1.99 cm², and 4.35%, respectively; Table S1 and Fig. S3).

Supplementary video related to this article can be found at http://dx.doi.org/10.1016/j.biomaterials.2017.02.007.

3.2. Long-term in vivo testing demonstrates well-functioning valves

We implanted the valves in the pulmonary position in sheep with 2 months (n=1, pilot), 6 months (n=5) and 12 (n=4) months follow-up. At termination, the valves showed good functionality with only mild central regurgitation (grade 1) and no stenosis (Fig. 2A–C, Table 2, and Supplementary Movies 2–5), with the exception of one of the 12-month explants (regurgitation grade 3). Invasive pressure measurements showed no gradient across the valves (Table 2). None of the animals showed any clinical signs of valve failure (e.g. murmur, dyspnea or ascites) during the complete

follow-up period.

Supplementary video related to this article can be found at http://dx.doi.org/10.1016/j.biomaterials.2017.02.007.

Macroscopically, all explanted valves showed pliable valve leaflets (Fig. 2D-I). In one of the 6-month explants and two of the 12-month explants, a small irregularity was observed at the free edge of one of the cusps, which did not affect functionality (Fig. 21). Average leaflet thickness was larger than native leaflet thickness and tended to increase from 6 to 12 months follow-up, although this increase was not statistically significant (Table 3). On average, no significant difference was detected in leaflet length between the 6- and 12-months explants (Table 3). However, one of the 12 months explants did show retraction of all cusps, leading to grade 3 regurgitation (Valve #12.4, Fig. 2]). This particular valve had displayed minor delamination of the polymeric leaflets prior to implantation. Pathological calcification was absent in all of the implanted valves, as assessed by careful visual inspection of the explants by the surgeons. Furthermore, no thromboembolic complications were observed and full autopsy revealed no valve-related thrombi or peripheral emboli (e.g. in lung tissue).

3.3. Scaffolds undergo extensive colonization by valvular interstitial-like cells and progressive endothelialization

Macrophages and neutrophilic granulocytes infiltrated abundantly throughout the porous microstructure of the scaffold, including the leaflet tip, already after 2 months. This was more pronounced in the 6-months explants and decreased from 6 to 12 months (Fig. 3A-H and Fig. S4). In addition, cells adhered onto the scaffold, forming a layer of neo-tissue, first on the pulmonary surface of the leaflet, and after 12 months also on the ventricular side. To assess cell phenotype, vimentin and α -SMA expression was evaluated. Pronounced vimentin expression was observed dispersed throughout the scaffold in both the 6- and 12-months explants (Fig. 3I–N). In contrast, α -SMA positive cells localized at the leaflet base and belly (Fig. 30, P), predominantly in the neotissue that had formed on the pulmonary side of the valve at 6 months follow-up. Importantly, after 12 months, α-SMA expression in the leaflet tended to be dampened, although this was not statistically significant (Fig. 30-Q), while vimentin expression remained abundant (Fig. 3J, M, N). CD45 positive cells were detected throughout the valve leaflets at both 6- and 12 months follow-up (Fig. S5).

Progressive endothelialization was evident from CD31 staining and SEM analysis (Fig. 4A—R). After 6 months, a progressive coverage of the pulmonary surface of the leaflet was observed (Fig. 4A—C), while on the ventricular surface, marked areas are visible in which the scaffold remained exposed, in particular near the free edge of the leaflet (Fig. 4K, M). At 12 months follow-up, endothelialization had developed into a fully confluent endothelial layer on the pulmonary surface (Fig. 4E—F) and a near-confluent endothelium on the ventricular surface (Fig. 4G), however with localized uncovered regions (Fig. 4H).

3.4. Native-like neo-tissue development is accompanied by gradual cell-driven scaffold resorption and functional mechanical behavior

Analogous to the cell colonization, profound valve remodeling was seen at the tissue level (Fig. 5A—N). At 6 months follow-up, collagen was mainly deposited as a neo-tissue layer onto the scaffold the pulmonary side of the leaflet. Minor collagen deposition was detected inside the scaffold, in particular near the hinge region, as evident from Masson's Trichrome and Picrosirius Red stainings (Fig. 5G—H, K-L). At 12 months follow-up, collagen deposition inside the scaffold was more pronounced, also in the belly region, and

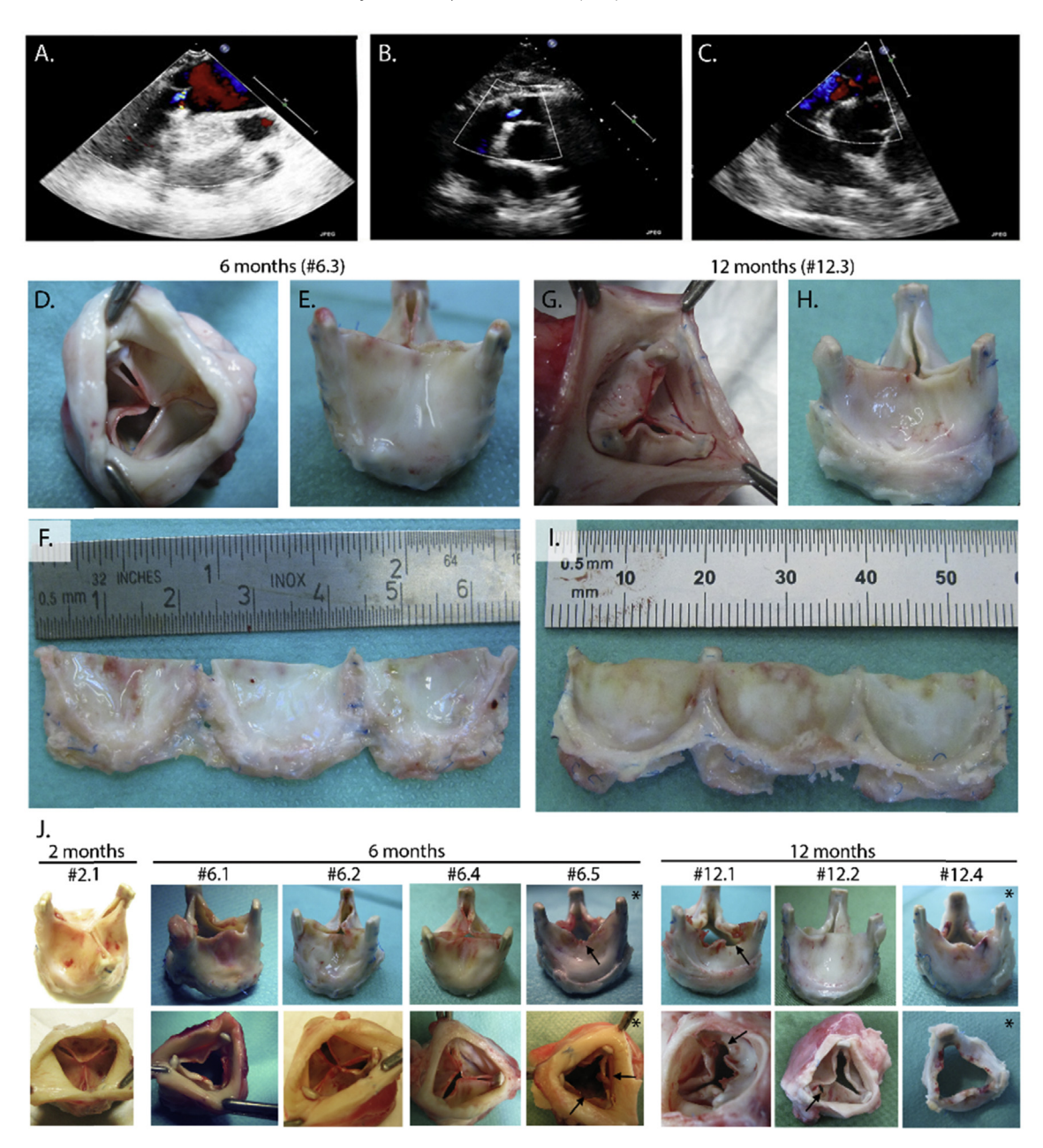


Fig. 2. In vivo functionality and gross morphology of explanted valves. (A-C) Echocardiography demonstrating good valve functionality with coapting leaflets (central regurgitation grade I) at 2 months (A), 6 months (B), and 12 months follow-up (C). (D-F) Gross appearance of representative valve after 6 months follow-up (valve #6.3). (G-I) Gross appearance of representative valve after 12 months follow-up (valve #12.3). (J) Gross appearance of valves after 2, 6, and 12 months follow-up. Arrows indicate irregularities in the valve leaflets. *indicates valves which displayed minor delamination of the synthetic scaffold prior to implantation (valves #6.5 and #12.4).

Table 2 *In vivo* hydrodynamic functionality of PC-BU valves.

		6 months	12 months
Insufficiency grade		1 (5 valves)	1 (3 valves), 3 (1 valve)
PVA		$2.58 \pm 0.29 \text{ cm}^2$	$2.72 \pm 0.24 \text{ cm}^2$
Systemic pressure	Systole	$93 \pm 12 \text{ mmHg}$	$85 \pm 20 \text{ mmHg}$
	Diastole	69 ± 15 mmHg	$55 \pm 15 \text{ mmHg}$
P _{RVOT}	Systole	15 ± 4 mmHg	$15 \pm 2 \text{ mmHg}$
	Diastole	$1.2 \pm 1 \text{ mmHg}$	$3 \pm 2 \text{ mmHg}$
P_{PA}	Systole	14.8 ± 3 mmHg	$15 \pm 3 \text{ mmHg}$
	Diastole	$2.6 \pm 1 \text{ mmHg}$	$7 \pm 3 \text{ mmHg}$
Transvalvular D P	Systole	$-0.2 \pm 5 \text{ mmHg}$	$0 \pm 3.6 \text{ mmHg}$
	Diastole	$1.4 \pm 1.4 \text{ mmHg}$	$4 \pm 3.6 \text{ mmHg}$

PVA, Pulmonary Valve Area; P_{RVOT} , pressure right ventricular outflow tract; P_{PA} , pressure pulmonary artery; $\Delta P = P_{PA} - P_{RVOT}$.

Table 3 Explant characteristics.

Property		PC-BU	6 months	12 months	Native
Leaflet length [mm]		_	9.7 ± 1.5	8.6 ± 2.1	_
Thickness [mm]	Hinge	0.4	1.1 ± 0.3	1.4 ± 0.5	0.29
	Belly	0.4	0.4 ± 0.04	0.8 ± 0.3	0.35
	Tip	0.4	0.7 ± 0.2	0.6 ± 0.3	0.24
Tangent Modulus [MPa]	Radial	3.0	5.2 ± 2.5	8.5 ± 0.6	1.3 ± 0.6
	Circumferential	4.1	4.9 ± 2.5	6.6 ± 2.7	3.7 ± 2.0
Molecular weight scaffold	M_n [kg/mol]	25.9 ± 0.1	19.5 ± 3.1	17.9 ± 4.1	_
	M_w [kg/mol]	57.6 ± 0.5	51.3 ± 5.6	48.4 ± 8.5	_
	D [-]	2.2 ± 0.02	2.7 ± 0.1	2.7 ± 0.2	_
DNA [µg/mg dry weight]	• •	_	6.5 ± 1.7	6.1 ± 2.1	8.2 ± 1.2
GAG [µg/mg dry weight]		_	27.5 ± 6.2	25.9 ± 2.2	47.9 ± 14.4
HYP [µg/mg dry weight]		_	22.6 ± 8.1	30.6 ± 5.1	37.0 ± 2.8
Elastin [µg/mg wet weight]		_	18.8	21.3 ± 1.4	22.4 ± 8.7

 M_n , number-averaged molecular weight; M_w , weight-averaged molecular weight; D_n , dispersity = M_w/M_n ; D_n ;

a remodeling region was observed near the hinge region (Fig. 5I–J, M–N). GAGs were observed in and on the scaffold at both the 6- and the 12-months explants, as evident from Pentachrome staining (Fig. 5A–F). Biochemical analysis revealed no significant differences in tissue composition between 6- and 12-months explants, although collagen content at 6 months was less than native (Fig. 5O–R). At 12 months follow-up, the tissue was composed of DNA, GAGs, collagen, and (tropo)elastin at concentrations comparable to the native pulmonary leaflet.

Expression of the (tropo)elastin protein strongly co-localized with collagen expression. To assess whether the deposited (tropo) elastin was incorporated into a functional fibrillar elastic matrix, co-staining of (tropo)elastin with the elastic matrix-forming proteins fibrillin-1 and fibrillin-2 was performed [40] (Fig. 6A–B). The 2 months explant displayed abundant fibrillin-1 expression throughout the leaflet, however coexpression with (tropo)elastin was limited to the hinge region (Fig. 6A). At 6 months, coexpression of fibrillin-1 and (tropo)elastin and mature elastic fibers were only detected on the pulmonary side of the leaflet. At 12 months, elastic fiber formation was observed on both sides of the leaflet, albeit more pronounced on the pulmonary side, as characterized by abundant coexpression of fibrillin-1 and (tropo)elastin, as well as mature fibers visible in the Pentachrome staining (Fig. 6C–E). On the ventricular side, elastic fiber formation was limited to the hinge region.

Analysis of the remaining polymer scaffold displayed a modest decrease in molecular weight, but a clear change in the molecular weight distribution (dispersity D), indicating that the remaining material has been affected (Fig. 7C-D and Table 3). Removal of tissue using sodium hypochlorite treatment showed that fibers that had been covered in tissue displayed clear signs of resorption, illustrated by cleaved fibers as well as surface erosion (Fig. 7B). Less-cellularized regions of scaffold, on the other hand, exhibited intact fibers without any signs of resorption (Fig. 7A). Histological analysis revealed that, after 12 months, the PC-BU had specifically disappeared from the section at the base of the leaflet, a section in which cells are relatively abundant (Fig. 3G and Fig. 5E, I, M). This tissue-dependent resorption was also reflected in the mechanical behavior of the explants (Fig. 7E-F). Starting from an almost linear elastic material behavior of the PC-BU starter matrix, the explanted valves displayed a more tissue-like non-linear elastic behavior, albeit with a higher stiffness compared to the native pulmonary valve (Table 3). In line with the absence of macroscopic pathological calcification, Alizarin Red staining displayed no expression in the 6months explants and two of the 12-months explants, and only very sparse spots in the other two 12-months explants were detected, localized near the leaflet base (Fig. S6).

4. Discussion

In situ TE using a cell free starter matrix is an emerging concept in the quest for developing living, adaptive heart valve prostheses that can last a lifetime. The starter matrix, or scaffold, can either be of natural origin, such as in the case of decellularized donor valves [19–21], decellularized SIS [14,15] or decellularized in vitro engineered heart valves [13,16–18], or of synthetic origin, as was applied in the present study of synthetic material-based in situ engineered heart valves. Our philosophy to use synthetic scaffolds is based on cost-effectiveness and high control over scaffold properties, which is paramount for valve functionality and the triggering of an appropriate regenerative response. This approach of synthetic biomaterial-based in situ TE has shown great potential when used as blood vessel replacement. Various studies have demonstrated successful preclinical application [26,27], leading to the first clinical trials as large replacement conduits in the low pressure circulation [41,42]. However, translation of these promising results in blood vessels to application as heart valve replacement is all but trivial, due to the stringent hemodynamic loading regime to which the heart valves are continuously exposed [22]. Here, we have described the development of a resorbable synthetic valve based on electrospun PC-BU, a supramolecular elastomeric material. The valves demonstrated sustained functionality over the 12 months follow-up period when implanted in the pulmonary position in sheep. Implanted valves were extensively colonized by host cells, throughout the entire leaflet. Endogenous neo-tissue was formed, replacing the initial synthetic scaffold, although scaffold degradation was not yet complete within 12 months follow-up. Notably, elastic fibers were detected, albeit sparse compared to the native leaflet and predominantly on the pulmonary side of the leaflet. Importantly, pathological calcification, the main risk factor for bioprosthetic heart valve prostheses, was absent throughout the 12 months implantation period. Together, these results present the initial proof-of-concept of in situ heart valve TE starting from a readily-available synthetic graft.

The strictly segmented molecular definition of PC-BU is not present in other synthetic elastomers that frequently have been employed for TE purposes. For example, poly(carbonate urethane) urea (PCUU) or poly(ester urethane)urea (PEUU), as well as the copolymers of these materials (see e.g. Hong et al. [43]) have a range in soft and hard block molecular identities. The sequence controlled nature of PC-BU translates into well-defined thermal and mechanical properties, and has the additional benefit that the degradation products of PC-BU will be limited in number and molecular variety. Moreover, as the individual macromolecules in PC-BU are very much alike, one may also expect a low distribution in their

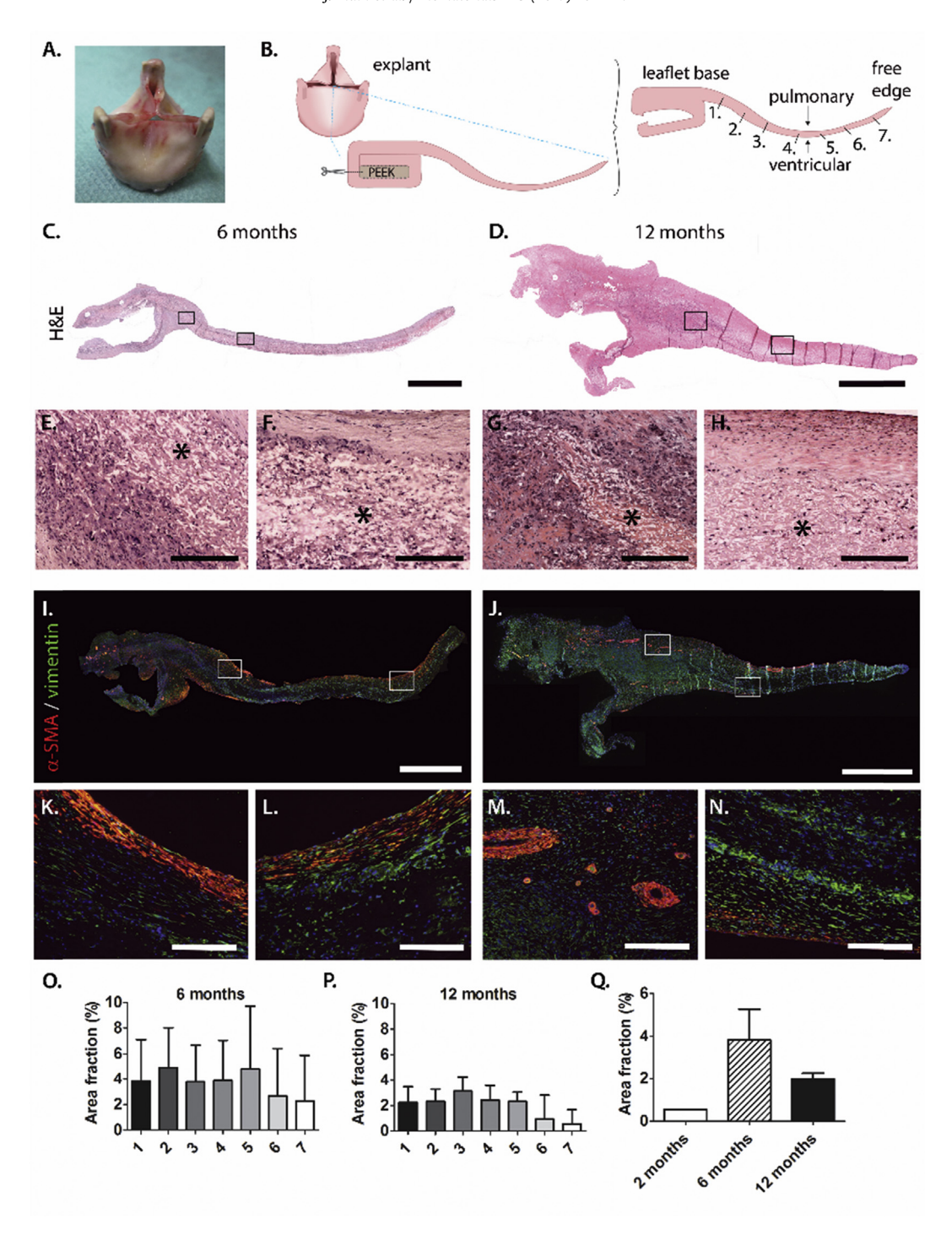


Fig. 3. In situ colonization of valves by host cells. (A,B) Explanted valves were cut longitudinally to obtain transections of the valve leaflets with orientation as indicated. (C-H) Valves were extensively colonized by host cells, infiltrating throughout the fibrous synthetic scaffold, as apparent in Hematoxylin and Eosin (H&E) staining. Displayed are tile scans of the entire leaflet (C,D) with zooms in the hinge and belly regions as indicated (E–H). Remnant scaffold fibers are visible in white (indicated by *). (I-N) Cells displayed vimentin (green) and α-Smooth Muscle Actin (α-SMA; red) expression. (O-P) Quantification of α-SMA staining in different locations of the leaflet, ranging from hinge = 1 to free edge = 7 (as indicated in B) and (O) the total α-SMA expression over the entire leaflet per time point. Displayed are the mean values + standard deviation. Scale bars, 1 mm (C-D, I-J) and 200 μm (E-H, K-N).

resorption rates. PC-BU is soluble in a range of organic solvents and solvent combinations enabling easy solvent processing by e.g. electrospinning. Finally, PC-BU is a thermoplastic elastomer that owes its elastomeric and tough qualities to the inter-chain supramolecular hydrogen bonding interactions between the butylene bis-urea groups. In this study we have used pristine PC-BU. However, for future modifications the supramolecular interactions

between the bis-urea groups can be employed to add function to the electrospun scaffold, for example by the inclusion of bioactive bis-urea peptides. This is analog to similar modular supramolecular approaches as recently reported [44,45]. The potential for biofunctionalization of the base material offers various opportunities for more personalized approaches, such as may be required for controlling neo-tissue formation in different age groups.

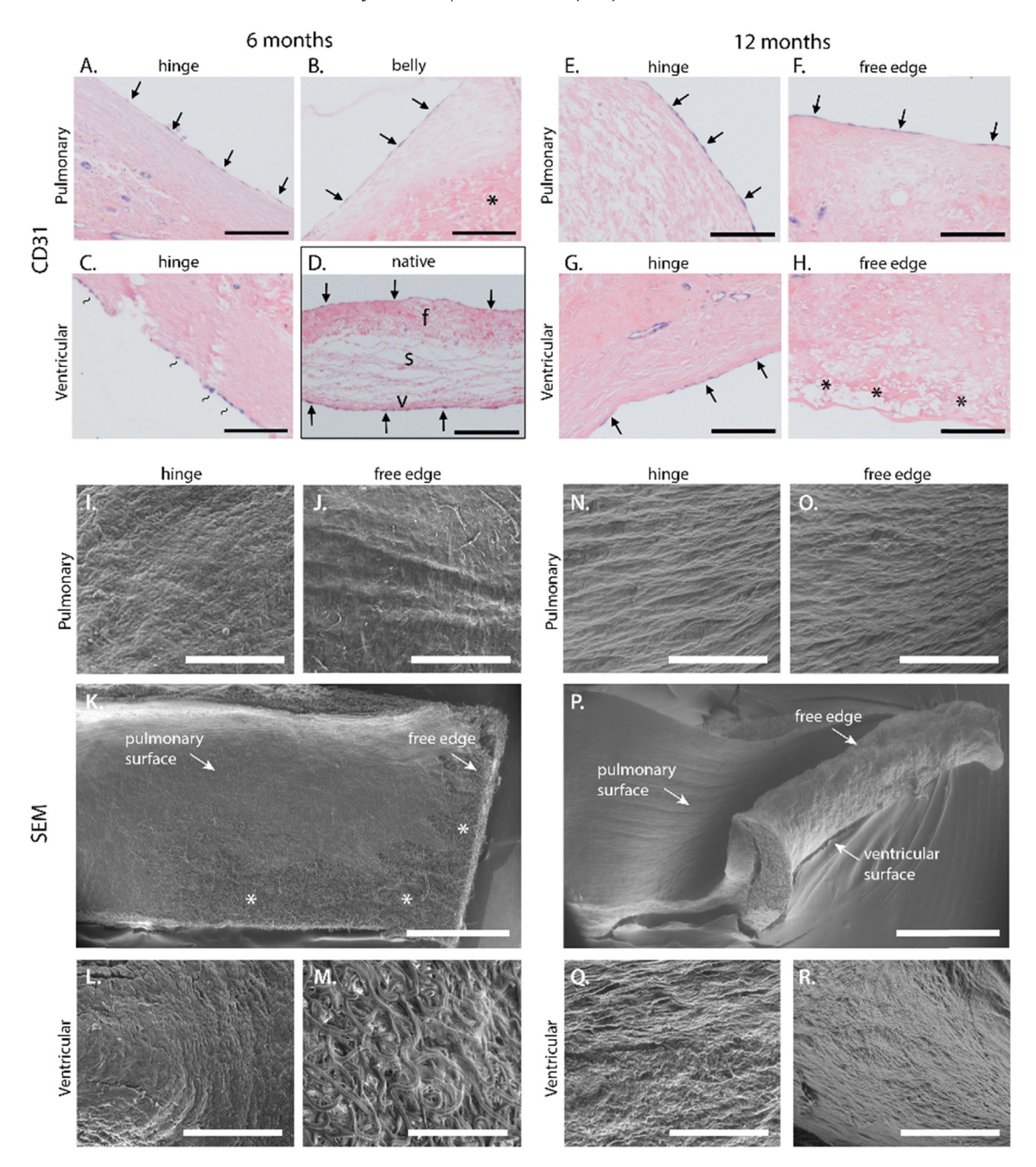


Fig. 4. Progressive *in situ* **endothelialization of the valves.** (**A-H**) CD31 staining of the explants and the native leaflet. After 6 months *in vivo*, endothelialization was predominantly observed on the pulmonary side of the leaflet (A, B; indicated by arrows), with expression comparable to the native leaflet (D; indicated by arrows; f = fibrosa, s = spongiosa, v = ventricularis). On the ventricular side, patchy endothelium was detected near the hinge region (C; indicated by ~), but not near the free edge. After 12 months, a near-confluent endothelial layer was observed on both the pulmonary and the ventricular surfaces (E-G; indicated by arrows), although localized uncovered regions were detected, mainly near the free edge (H; indicated by *). (**I-R**) Scanning electron microscopy (SEM) analysis displays progressive coverage of the scaffold surface. Displayed are representative overview images of the valve leaflets (K,P; * indicate uncovered scaffold regions), and details of regions near the hinge and the free edge of the pulmonary (I,J,N,O) and ventricular surface (L,M,Q,R). Scale bars, 200 μm (A–H); 100 μm (I-J, L-O, Q-R), and 1 mm (K,P).

Microstructurally, the valves consisted of microfibers and, consequently, a large pore size, which is previously reported to be stimulatory for cellular infiltration, endogenous matrix production, and regenerative remodeling [28–30]. The origin of colonizing cells could not be fully determined within the current study setup. Based on the present data, however, we speculate that cellular colonization of the scaffolds in the sheep model occurred via two routes: cell recruitment from the circulatory system and tissue in- and overgrowth from the valve root, both of which have been described to occur in material-based *in situ* tissue-engineered blood vessels

[28,46]. CD45 staining indicate a role for circulatory immune cells, such as monocytes (Fig. S5). Concurrently, macrophage presence was evident from histological analysis. Rather than trying to avoid an inevitable immunogenic response, our philosophy is to make use of and harness the natural foreign body response to induce regeneration [19,20,23]. Correspondingly, macrophages have been proposed to play a pivotal role in the regenerative cascade [47], and their phenotypical state can be modulated via the scaffold biophysical properties [48], as well as by the hemodynamic loads on the valve [30,49]. A more detailed, antibody-based characterization

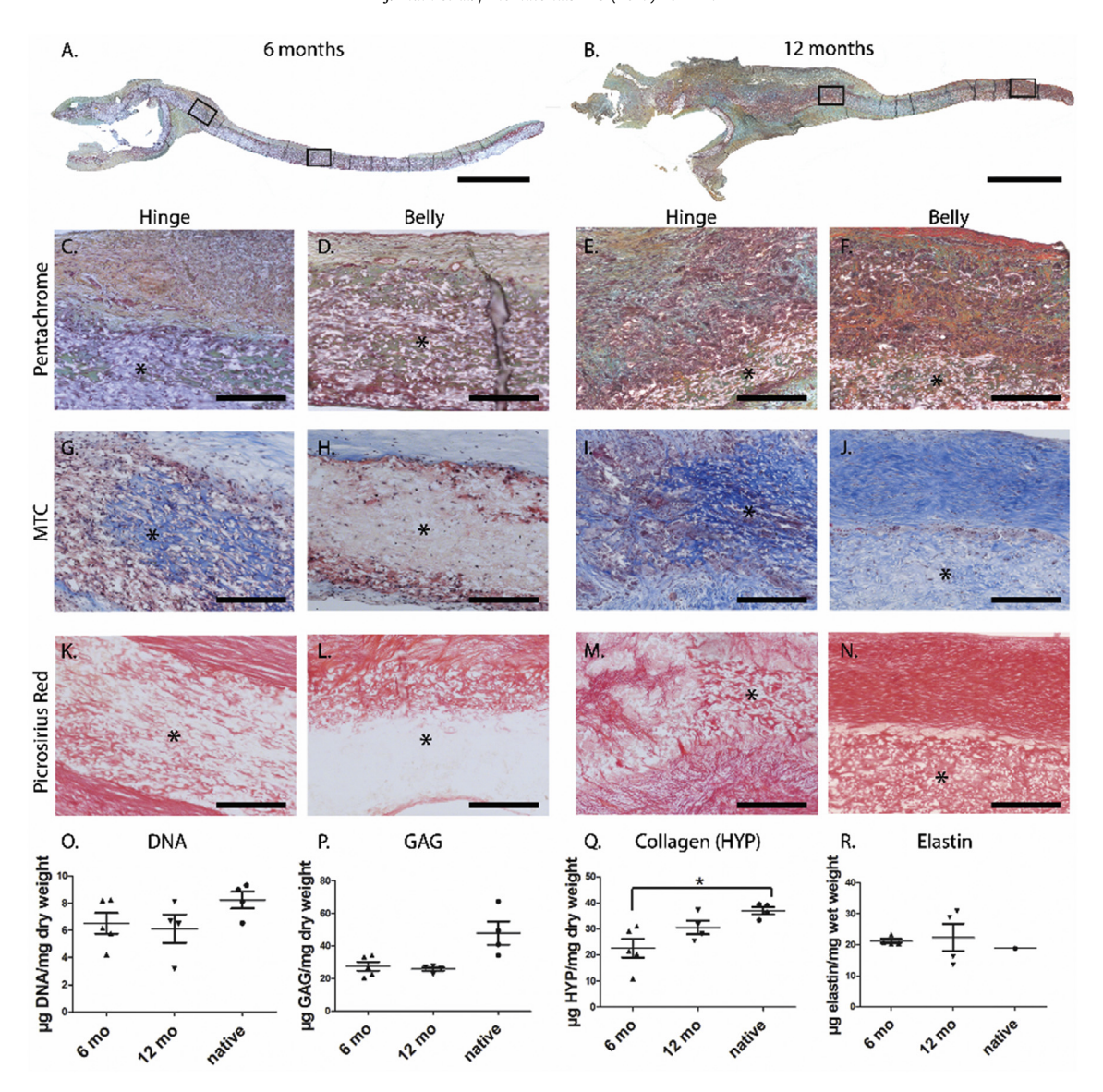


Fig. 5. Formation and composition of neo-tissue. (A-F) Rusell-Movat Pentachrome staining on the explants after 6 and 12 months (collagen in yellow, cell nuclei in dark red, elastin fibers in black, muscle tissue in red, and glycosaminoglycans in blue-green). Displayed are longitudinal sections of the entire valve leaflet (A,B), with zooms in the hinge and belly regions as indicated (C-F). (G-J) Masson's Trichrome (MTC) stain in the hinge and belly regions of 6- and 12-month explants (collagen in red). *indicates remaining scaffold. Scale bars, 1 mm (A,B) and 200 μ m (C-N). (G-R) Biochemical composition of the explanted leaflets, in terms of DNA, glycosaminoglycans (GAG), hydroxyproline (HYP), and elastin. Data represent mean \pm standard error of the mean, with n=5 for 6 months, n=4 for 12 months, and n=4 for native (DNA, GAG, HYP) or n=1 for native (elastin). The native elastin (n=1) was not included in statistical analysis. *P < 0.05.

of spatio-temporal macrophage infiltrates in our valves would greatly contribute to our understanding of the observed phenomena. However, macrophage behavior is subject to large interspecies differences and appropriate phenotypical markers have not been described for the ovine model. As such, we excluded CD68 (a human pan-macrophage marker) and EMR1 (Epidermal growth factor-like module-containing Mucin-like hormone Receptor-like1; the human homolog of the murine macrophage marker F4/80) as appropriate macrophage markers for the ovine model after careful evaluation. Extensive investigation of the cellular and molecular mechanisms underlying neo-tissue formation, and the origin of colonizing cells (i.e. using tracing studies), is our next step towards mechanistic understanding and may provide essential insights to adjust regenerative processes via scaffold modifications.

The newly formed valve tissue demonstrated an increasingly mature organization, with presence of collagen, GAGs, and elastin. Most remarkable is the formation of mature elastic fibers in the valve leaflet, in the presence of the microfibrils fibrillin-1 and fibrillin-2. The presence of a proper elastic network is essential to long-term functioning of the valve [50,51]. The de novo formation of mature elastic fibers in (tissue) engineered valves has been a major challenge, in particular for *in vitro* approaches [22]. The formation of functional elastic fibers is a complex process which requires the incorporation of tropoelastin into a microfibrillar network, consisting of fibrillin-1, fibrillin-2, as well as other proteins such as cross-linkers [40]. Recent work by Votteler et al. describes the spatiotemporal expression of these proteins during early valve development, revealing that expression of fibrillin-1 and -2 precedes elastin expression [51]. Since the elastin assay and elastin antibody stainings do not distinguish between tropoelastin and mature elastin, we assessed the formation of elastic fibers by analyzing the coexpression of (tropo)elastin with the essential

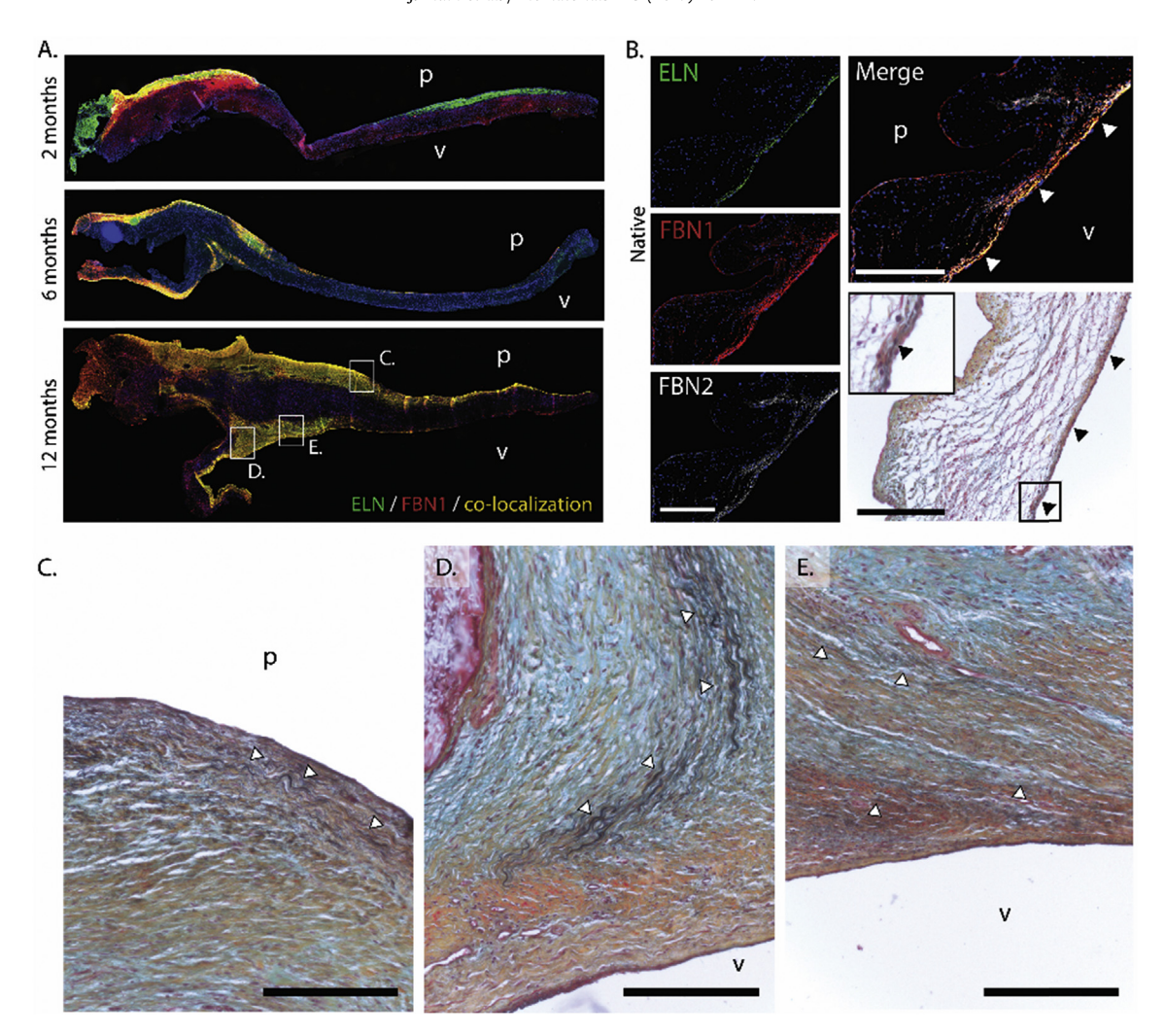


Fig. 6. Elastic fiber formation. (A) Immunofluorescent staining of Elastin protein (ELN; green), Fibrillin-1 (FBN1; red) and cell nuclei (DAPI; blue) for the 2, 6, and 12 months explants. Colocalization of ELN and FBN1 appears in yellow. Displayed are merged tile scans of the entire leaflet. (B) Elastin fibers in the native sheep pulmonary leaflet. Displayed are immunofluorescent images of ELN (green), FBN1 (red), and Fibrillin-2 (FBN2; white), with a merged overlay image, and Pentachrome staining. Expression of black elastin fibers in the Pentachrome staining on the ventricular surface of the leaflet corresponds to colocalization of ELN, FBN1, and FBN2 in the merged immunofluorescent image (indicated by triangles). (C-E) Details of the 12 month explant (Pentachrome staining) at the pulmonary surface (C) and the ventricular surface near the hinge (D,E). Elastic fibers appear in black (indicated by triangles). p and v indicate the pulmonary and ventricular side of the leaflet, respectively. Scale bars, 200 μm.

microfibrils fibrillin-1 and fibrillin-2. This was cross-referenced with the Pentachrome staining, which strictly stains positive for mature elastic fibers (in black), but not tropoelastin or immature fibers. Despite native-like levels of (tropo)elastin, the amount of mature elastic fibers in the PC-BU explants was still limited compared to the native pulmonary valve at 12 months follow-up. Nevertheless, the development of elastic fibers in our valves is of paramount importance and it is exemplary for the maturity and functionality of the newly formed tissue.

Moreover, similar to the native valve, the tissue displays a certain level of layeredness. This is likely to be a direct effect of the hemodynamic loads, and in particular the shear stresses on the valve, given the pronounced early tissue formation on the fibrosa side, in contrast to the ventricular side of the leaflet. Similar to the neo-tissue formation, endothelialization of the ventricular surface of the valve leaflet was clearly slower compared to the pulmonary surface, suggesting shear stress dependent endothelialization of the scaffolds. These results point at a potential role for endothelial-to-mesenchymal transformation, as this is known to be shear stress-dependent [52], although this was not and could not be evaluated with the current dataset. At 12 months follow-up,

endothelialization was near-complete. Importantly, no thromboembolic events (a common issue for traditional heart valve prostheses) were observed and no emboli were detected in peripheral organs, although the animals were on a mild anticoagulation regimen of acetylsalicylic acid. Another key finding is the absence of pathological calcification and chronic inflammation. Calcification is one of the main complications for any bioprosthetic valve prosthesis. In particular in the sheep model, which is the designated animal model for heart valve prostheses given its increased tendency for calcification. We speculate that the use of fibrin gel may have had a beneficial biological role in the prevention of thrombosis and inflammation-induced calcification. Mature, cross-linked fibrin is known to be relatively non-thrombogenic [53]. Moreover, a recent study by Hsieh et al. proposes that fibrin has a strong antiinflammatory effect on macrophages, even in a highly proinflammatory biochemical environment [54]. Absence of calcification, even in the worst-case scenario that is the sheep model, may be predictive for successful long-term functionality of the valve. However, since our current data does not extend beyond the 12 months follow-up and the scaffold resorption had not been complete at this time point, a longer term follow-up study is warranted

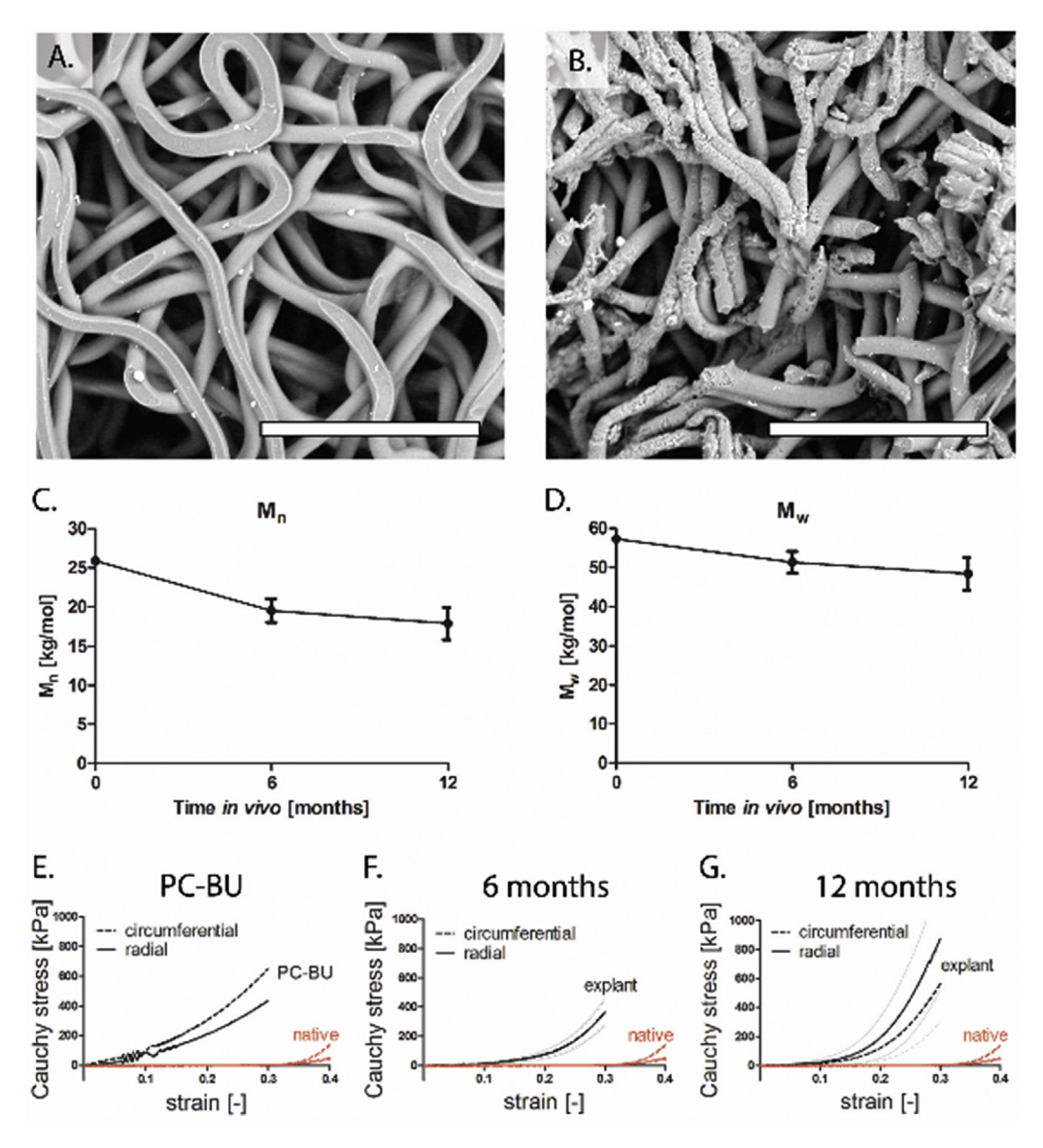


Fig. 7. Scaffold degradation and changes in mechanical properties. (A,B) Representative scanning electron microscopy (SEM) images of 6-month explants. Before SEM, the tissue was removed by sodium hypochlorite treatment in order to expose the degrading scaffold fibers. Images shown are from a cell-poor region in which fibers remained intact (A) and a cell-rich region in which fibers were clearly affected by cell-driven resorption (B). Scale bars, 50 μ m. (C,D) Molecular weight of the remaining scaffold material as determined by Gel Permeation Chromatography. Displayed are mean \pm standard error of the mean. (E-G) Biaxial tensile tests on the PC-BU valve leaflet prior to implantation and on the 6- and 12-months explants, in comparison with the native leaflet (in red). Data represent mean (black lines) \pm standard error of the mean (grey lines), with n = 1 for PC-BU, n = 5 for 6 months, and n = 2 for 12 months. (For interpretation of the references to colour in this figure legend, the reader is referred to the web version of this article.)

to validate true long-term functionality.

With increasing tissue formation, some valves showed thickening and the development of a microvasculature near the leaflet root. Although neovascularization is necessary for mature tissue formation, these observations could also be considered a potential risk [55]. Yet, decreasing α -SMA expression at 12 months follow-up indicates that progressive leaflet thickening beyond this moment is unlikely to occur. Progressive leaflet thickening and subsequent retraction is the common mode of failure for tissue-engineered valves, caused by persistent α -SMA expression of activated myofibroblasts [12,13]. In contrast, the observed dampening of α -SMA expression with retained vimentin expression is indicative of the phenotypical transition from activated VICs to quiescent VICs [56], marking a state of tissue homeostasis, essential to long-term functioning of the valve. Albeit requiring further investigation at longer follow-up times, the currently achieved state of VIC

quiescence is a promising indicator that leaflet retraction will not occur upon further resorption of the scaffold. Among the 12-month explants we found one valve as an outlier in terms of leaflet remodeling and functionality (pulmonary insufficiency grade 3). This reduced function could be attributed to delamination of the polymeric starter matrix for this particular valve, which was also observed for one of the 6-months valves (Fig. 2] and Fig. S4). Upon explantation, both these valves displayed increased α-SMA expression and excessively thick tissue compared to the other valves. Although marginal delamination of the scaffold was observed prior to implantation of these valves, no in vivo side effects were anticipated. Similar large variations in long-term in vivo outcome, even in healthy laboratory animals, have recently been reported for in situ tissue engineered blood vessels [57]. These observations warrant protocolled and standardized procedures for scaffold manufacturing and quality testing.

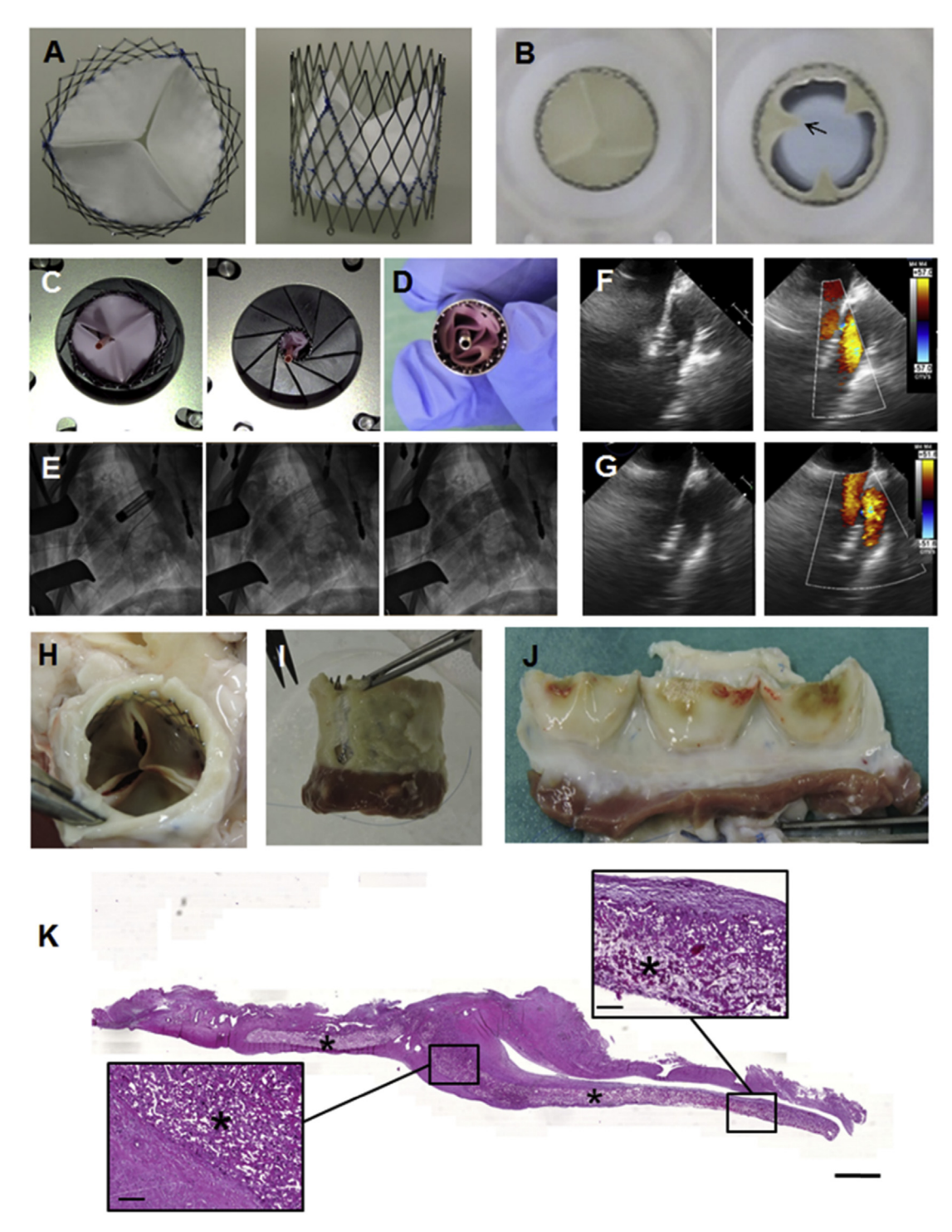


Fig. 8. Feasibility of minimally invasive implantation of the novel PC-BU valve, from *in vitro* to 6 months *in vivo*. As an initial assessment of the feasibility of minimally-invasive implantation of the novel PC-BU valves, the PC-BU valves were sutured onto a Nitinol stent and delivered transapically as pulmonary valve replacements in five adult sheep (n = 5; weight range of $56.4 \pm 3.9 \text{ kg}$), with a planned follow-up of 1 months (n = 2) and 6 months (n = 3). All animals (n = 5) received human care and the study was approved by the ethics committee (Veterināramt, Gesundheitsdirektion, Kanton Zürich ZH_09_2014) in compliance with the Guide for the Care and Use of Laboratory Animals, published by the National Institutes of Health (NIH publication No. 85-23). (A) Top view and side photographs of the PC-BU valve sutured on the Nitinol stent (\emptyset = 28 mm). (B) Movie stills of the *in vitro* functionality test demonstrating correct valve functionality despite the bending of the central part of the leaflets (arrow). (C) Photographs of the valve before and after crimping, with a diameter change from 28 mm to 10 mm. (D) Distal view of the valve loaded into the delivery capsule. (E) Implantation angiography with positioning of the capsule, valve deployment, and assessment of valve functionality. In brief, after a right-sided thoracotomy, the pericardium was opened and the right ventricle (RV) was exposed for transapical access. Felt enforced purse-string sutures (Prolene 3-0) were placed, the RV was punctured and a guide wire was placed into the pulmonary artery. Next, the pulmonary root was visualized and in parallel the stented valves were crimped and loaded onto a custom-made, pressure-based delivery system (OD = 10 mm). Thereafter, the delivery system was inserted into the RV and advanced into the pulmonary artery. (F) Echocardiography demonstrated instant valve functionality post-delivery, which was then maintained (G) up to 6 months post implantation, with no signs of regurgitation. Gross appearance of the

Pivotal to our approach is the resorption mechanism of the scaffold. Whereas fast resorption has been suggested to be key to successful in situ regeneration of blood vessels [26], we pose that the safe regeneration of a functioning heart valve requires a more tailored approach. Previous studies attempting in situ TE of heart valves using rapidly-degrading polyglycolic acid-based valves resulted in inadequate tissue formation and subsequent valve failure [58]. In contrast, here we employed the slow-resorbable supramolecular elastomer PC-BU. Detailed characterization of the resorption mechanisms revealed that this polymer is prone to both oxidative and enzymatic resorption, but relatively stable in comparison to polyester-based supramolecular materials [35] (Supplemental Dataset 1). We observed that scaffold resorption had not completed after 12 months in vivo, and full transformation into an autologous living valve had not yet completed. Most importantly, however, resorption was observed to be cell-driven. The highly cellularized regions at the leaflet base demonstrated increased and even near-complete levels of resorption, while being rich in new tissue. In less cellularized regions, such as the leaflet belly, on the other hand, scaffold fibers remained intact. This co-localization of tissue formation and scaffold resorption means that tissue regeneration is safe: the structural integrity of the valve is warranted at all times. Fine-tuning of the resorption rate in relation to the patient target group (e.g. growing infants) can be achieved via modification of the material, for example by optional mixing-in of bioactive bis-ureas that may regulate degradation properties.

As with any new technology, several challenges remain to be overcome. Clearly, the use of a PEEK supporting ring is still suboptimal and could be replaced by a degrading ring or stent for future applications. As an alternative first step, we therefore integrated the scaffolds into self-expandable nitinol stents (length 38 mm, outer diameter 28 mm) for minimally invasive transapical delivery. Although detailed evaluation is topic of current studies, preliminary results demonstrate that transapical delivery of these novel valves is indeed feasible, with successful functionality up to 6 months follow-up in sheep (Fig. 8). Another challenge lies in the application of the current valve in the aortic position. In vitro functionality in aortic conditions confirmed that the bare PC-BU valve is fully functional up to an equivalent of 4 weeks in vivo. This is not taking into account the *in vivo* remodeling and based on predictive numerical models we anticipate that regeneration of the valve in aortic conditions would indeed be possible [59].

In conclusion, this study demonstrates proof-of-concept of the *in situ* transformation of a bioresorbable polymer graft into an autologous pulmonary heart valve in the complex hemodynamic environment of the heart. Long-term valve function was good and graft remodeling resulted in valvular tissue with an unprecedented maturity and stability, towards native organization and mechanical behavior. Compared to other *in situ* valve TE approaches the technology does not require any donor tissue or cells and is competitive in terms of costs, logistics and regulation. More importantly, the designed supramolecular elastomer offers the potential to strictly control graft mechanical, degradation and bioactive properties. Herein lies the full potential and benefit of the chosen material-driven approach.

Author contributions

J.K., H.T. and M.Y.E. designed *in vivo* experiments, implanted the grafts, and performed *in vivo* functionality measurements. S.H.M.S. and H.M.J. designed and prepared the material and with P.Y.W.D. performed chemical analyses of the graft and explants. R.D. created the valve graft and performed *in vitro* performance tests. M.C.P.B. performed graft resorption and SEM studies and oversaw electrospinning. M.W.T.J. performed mechanical and biochemical

characterization of grafts and explants and analyzed data with A.I.P.M.S. A.V., H.T. and S.D. performed and analyzed histology of the explants. M.Y.E., E.S.F, P.E.D, and V.L. planned the transcathether experiments, and performed and analyzed histology of the explants. S.D. and A.I.P.M.S. performed matrix analysis and (immuno) histology. F.P.T.B., S.P.H. and C.V.C.B. designed and oversaw the studies. All authors interpreted results and contributed to the manuscript; J.K., H.T., A.I.P.M.S, P.Y.W.D., H.M.J., M.Y.E and C.V.C.B prepared the manuscript.

Disclosures

M.C.P.B. is employed by Xeltis BV. F.P.T.B., C.V.C.B., and S.P.H. are shareholders of Xeltis BV. S.H.M.S. and H.M.J. are employed by SyMO-Chem BV. J.K., H.T., A.I.P.M.S., M.Y.E., E.S.F., P.E.D., R.D., S.D., M.W.J.T.J.-B., V.L., A.V., and P.Y.W.D. report that they have no competing interests.

Acknowledgments

We thank G. van Almen for performing cytotoxicity tests, B. Sanders for mechanical testing of scaffolds and heart valves, J.W. van Rijswijk for assistance with histology, E. Caliskan for assistance with transcatheter implantations, and M. Uiterwijk for assistance with echocardiography. We are very grateful to E. Aikawa for thorough discussions on histological research output and we greatly appreciate the fruitful collaborations of the iValve team members, including M. Cox, M. Verhaar, E. Meijer, A. Bosman, M. Post, and A. Driessen-Mol.

This research forms part of Project P1.01 iValve of the research program of the BioMedical Materials institute, co-funded by the Dutch Ministry of Economic Affairs (Grant number DHF-2008T089), and of project iValve-II, powered by Health-Holland, top sector of Life Science and Health (Grant number TTT11403B), supported by the Dutch Ministry of Economic Affairs. The financial contribution of the Dutch Heart Foundation is gratefully acknowledged.

Appendix A. Supplementary data

Supplementary data related to this article can be found at http://dx.doi.org/10.1016/j.biomaterials.2017.02.007.

References

- [1] R. El Oakley, P. Kleine, D.S. Bach, Choice of prosthetic heart valve in today's practice, Circulation 117 (2008) 253–256, http://dx.doi.org/10.1161/ CIRCULATIONAHA.107.736819.
- [2] M. Ruel, A. Kulik, B.K. Lam, F.D. Rubens, P.J. Hendry, R.G. Masters, et al., Long-term outcomes of valve replacement with modern prostheses in young adults, Eur. J. Cardio-Thoracic Surg. 27 (2005) 425–433, http://dx.doi.org/10.1016/j.ejcts.2004.12.002.
- [3] K. Hammermeister, G.K. Sethi, W.G. Henderson, F.L. Grover, C. Oprian, S.H. Rahimtoola, Outcomes 15 years after valve replacement with a mechanical versus a bioprosthetic valve: final report of the Veterans Affairs randomized trial, J. Am. Coll. Cardiol. 36 (2000) 1152–1158, http://dx.doi.org/ 10.1016/S0735-1097(00)00834-2.
- [4] I. El-Hamamsy, Z. Eryigit, L.-M. Stevens, Z. Sarang, R. George, L. Clark, et al., Long-term outcomes after autograft versus homograft aortic root replacement in adults with aortic valve disease: a randomised controlled trial, Lancet 376 (2010) 524–531, http://dx.doi.org/10.1016/S0140-6736(10)60828-8.
- [5] J.P. Puvimanasinghe, J.J.M. Takkenberg, M.B. Edwards, M.J.C. Eijkemans, E.W. Steyerberg, L.A. Van Herwerden, et al., Comparison of outcomes after aortic valve replacement with a mechanical valve or a bioprosthesis using microsimulation, Heart 90 (2004) 1172–1178, http://dx.doi.org/10.1136/ hrt.2003.013102.
- [6] M.H. Yacoub, J.J.M. Takkenberg, Will heart valve tissue engineering change the world? Nat. Clin. Pract. Cardiovasc Med. 2 (2005) 60–61, http://dx.doi.org/ 10.1038/ncpcardio0112.
- [7] J.E. Mayer, In search of the ideal valve replacement device, J. Thorac. Cardiovasc Surg. 122 (2001) 8–9, http://dx.doi.org/10.1067/mtc.2001.115926.

- [8] S.P. Hoerstrup, R. Sodian, S. Daebritz, J. Wang, E.A. Bacha, D.P. Martin, et al., Functional living trileaflet heart valves grown in vitro, Circulation 102 (2000) III44—III49, http://dx.doi.org/10.1161/01.CIR.102.suppl_3.III-44.
- [9] T. Shin'oka, D. Shum-Tim, P.X. Ma, R.E. Tanel, N. Isogai, R. Langer, et al., Creation of viable pulmonary artery autografts through tissue engineering. J. Thorac. Cardiovasc Surg. 115 (1998) 536–545, http://dx.doi.org/10.1016/S0022-5223(98)70315-0 discussion 545–6.
- [10] T.C. Flanagan, J.S. Sachweh, J. Frese, H. Schnöring, N. Gronloh, S. Koch, et al., In vivo remodeling and structural characterization of fibrin-based tissueengineered heart valves in the adult sheep model, Tissue Eng. Part A 15 (2009) 2965–2976. http://dx.doi.org/10.1089/ten.TEA.2009.0018.
- [11] T. Shin'oka, P.X. Ma, D. Shum-Tim, C.K. Breuer, R.A. Cusick, G. Zund, et al., Tissue-engineered heart valves. Autologous valve leaflet replacement study in a lamb model, Circulation 94 (1996) II164—II168, http://dx.doi.org/10.1016/ 0003-4975(95)00733-4.
- [12] D. Gottlieb, T. Kunal, S. Emani, E. Aikawa, D.W. Brown, A.J. Powell, et al., In vivo monitoring of function of autologous engineered pulmonary valve, J. Thorac. Cardiovasc Surg. 139 (2010) 723–731, http://dx.doi.org/10.1016/j.jtcvs. 2009 11 006
- [13] A. Driessen-Mol, M.Y. Emmert, P.E. Dijkman, L. Frese, B. Sanders, B. Weber, et al., Transcatheter implantation of homologous "off-the-shelf" tissue-engineered heart valves with self-repair capacity: long-term functionality and rapid in vivo remodeling in sheep, J. Am. Coll. Cardiol. 63 (2014) 1320—1329, http://dx.doi.org/10.1016/j.jacc.2013.09.082.
- [14] F. Zafar, R.B. Hinton, R.A. Moore, R.S. Baker, R. Bryant, D.A. Narmoneva, et al., Physiological growth, remodeling potential, and preserved function of a novel bioprosthetic tricuspid valve: tubular bioprosthesis made of small intestinal submucosa-derived extracellular matrix, J. Am. Coll. Cardiol. 66 (2015) 877–888, http://dx.doi.org/10.1016/j.jacc.2015.06.1091.
- [15] C.E. Ruiz, M. Iemura, S. Medie, P. Varga, W.G. Van Alstine, S. Mack, et al., Transcatheter placement of a low-profile biodegradable pulmonary valve made of small intestinal submucosa: a long-term study in a swine model, J. Thorac. Cardiovasc Surg. 130 (2005) 477–484, http://dx.doi.org/10.1016/ i.ircvs.2005.04.008.
- [16] B. Weber, P.E. Dijkman, J. Scherman, B. Sanders, M.Y. Emmert, J. Grünenfelder, et al., Off-the-shelf human decellularized tissue-engineered heart valves in a non-human primate model, Biomaterials 34 (2013) 7269–7280, http://dx.doi.org/10.1016/j.biomaterials.2013.04.059.
- [17] J.M. Reimer, Z.H. Syedain, B.H.T. Haynie, R.T. Tranquillo, Pediatric tubular pulmonary heart valve from decellularized engineered tissue tubes, Biomaterials 62 (2015) 88–94, http://dx.doi.org/10.1016/j.biomaterials. 2015.05.009
- [18] Z. Syedain, J. Reimer, J. Schmidt, M. Lahti, J. Berry, R. Bianco, et al., 6-Month aortic valve implantation of an off-the-shelf tissue-engineered valve in sheep, Biomaterials 73 (2015) 175–184, http://dx.doi.org/10.1016/ j.biomaterials.2015.09.016.
- [19] K. Theodoridis, I. Tudorache, A. Calistru, S. Cebotari, T. Meyer, S. Sarikouch, et al., Successful matrix guided tissue regeneration of decellularized pulmonary heart valve allografts in elderly sheep, Biomaterials 52 (2015) 221–228, http://dx.doi.org/10.1016/j.biomaterials.2015.02.023.
- [20] I. Tudorache, K. Theodoridis, H. Baraki, S. Sarikouch, C. Bara, T. Meyer, et al., Decellularized aortic allografts versus pulmonary autografts for aortic valve replacement in the growing sheep model: haemodynamic and morphological results at 20 months after implantation, Eur. J. Cardio-Thoracic Surg. 49 (2016) 1228–1238, http://dx.doi.org/10.1093/ejcts/ezv362.
- [21] L. Iop, A. Bonetti, F. Naso, S. Rizzo, S. Cagnin, R. Bianco, et al., Decellularized allogeneic heart valves demonstrate self-regeneration potential after a longterm preclinical evaluation, PLoS One (2014) 9, http://dx.doi.org/10.1371/ journal.pone.0099593.
- [22] A. Mol, A.I.P.M. Smits, C.V.C. Bouten, F.P.T. Baaijens, Tissue engineering of heart valves: advances and current challenges, Expert Rev. Med. Devices 6 (2009) 259–275, http://dx.doi.org/10.1586/erd.09.12.
- [23] C.V.C. Bouten, A. Driessen-Mol, F.P.T. Baaijens, In situ heart valve tissue engineering: simple devices, smart materials, complex knowledge, Expert Rev. Med. Devices 9 (2012) 453–455, http://dx.doi.org/10.1586/erd.12.43.
- [24] S.L.M. van Loon, A.I.P.M. Smits, A. Driessen-Mol, F.P.T. Baaijens, C.V.C. Bouten, The immune response in in situ tissue engineering of aortic heart valves, in: E. Aikawa (Ed.), Calcif. Aortic Valve Dis., Rijeka: InTech, 2013, pp. 207–245, http://dx.doi.org/10.5772/54354.
- [25] A.K. Capulli, L.A. MacQueen, S.P. Sheehy, K.K. Parker, Fibrous scaffolds for building hearts and heart parts, Adv. Drug Deliv. Rev. 96 (2016) 83–102, http://dx.doi.org/10.1016/j.addr.2015.11.020.
- [26] W. Wu, R a Allen, Y. Wang, Fast-degrading elastomer enables rapid remodeling of a cell-free synthetic graft into a neoartery, Nat. Med. 18 (2012) 1148–1153, http://dx.doi.org/10.1038/nm.2821.
- [27] J.D. Roh, R. Sawh-Martinez, M.P. Brennan, S.M. Jay, L. Devine, D a Rao, et al., Tissue-engineered vascular grafts transform into mature blood vessels via an inflammation-mediated process of vascular remodeling, Proc. Natl. Acad. Sci. U. S. A. 107 (2010) 4669–4674, http://dx.doi.org/10.1073/pnas.0911465107.
- [28] H. Talacua, A.I.P.M. Smits, D.E.P. Muylaert, J.W. van Rijswijk, A. Vink, M.C. Verhaar, et al., In situ tissue engineering of functional small-diameter blood vessels by host circulating cells only, Tissue Eng. Part A 21 (2015) 2583—2594, http://dx.doi.org/10.1089/ten.TEA.2015.0066.
- [29] A. Balguid, A. Mol, M.H. van Marion, R.A. Bank, C.V.C. Bouten, F.P.T. Baaijens, Tailoring fiber diameter in electrospun poly(epsilon-caprolactone) scaffolds

- for optimal cellular infiltration in cardiovascular tissue engineering, Tissue Eng. Part A 15 (2009) 437–444, http://dx.doi.org/10.1089/ten.tea.2007.0294.
- [30] V. Ballotta, A. Driessen-Mol, C.V.C. Bouten, F.P.T. Baaijens, Strain-dependent modulation of macrophage polarization within scaffolds, Biomaterials 35 (2014) 4919–4928, http://dx.doi.org/10.1016/j.biomaterials.2014.03.002.
- [31] A. Mol, M.C.M. Rutten, N.J.B. Driessen, C.V.C. Bouten, G. Zünd, F.P.T. Baaijens, et al., Autologous human tissue-engineered heart valves: prospects for systemic application, Circulation 114 (2006) 1152–1158, http://dx.doi.org/10.1161/ CIRCULATIONAHA.105.001123.
- [32] A. Mol, M.I. van Lieshout, C.G. Dam-de Veen, S. Neuenschwander, S.P. Hoerstrup, F.P.T. Baaijens, et al., Fibrin as a cell carrier in cardiovascular tissue engineering applications, Biomaterials 26 (2005) 3113–3121, http:// dx.doi.org/10.1016/j.biomaterials.2004.08.007.
- [33] E. Wisse, A.J.H. Spiering, E.N.M. van Leeuwen, R.A.E. Renken, P.Y.W. Dankers, L.A. Brouwer, et al., Molecular recognition in poly(epsilon-caprolactone)based thermoplastic elastomers, Biomacromolecules 7 (2006) 3385–3395, http://dx.doi.org/10.1021/bm060688t.
- [34] E. Wisse, L.E. Govaert, H.E.H. Meijer, E.W. Meijer, Unusual tuning of mechanical properties of thermoplastic elastomers using supramolecular fillers, Macromolecules 39 (2006) 7425–7432, http://dx.doi.org/10.1021/ma060986i.
- [35] M.C.P. Brugmans, S.H.M. Söntjens, M. a. J. Cox, A. Nandakumar, A.W. Bosman, T. Mes, et al., Hydrolytic and oxidative degradation of electrospun supramolecular biomaterials: in vitro degradation pathways, Acta Biomater. 27 (2015) 21–31, http://dx.doi.org/10.1016/j.actbio.2015.08.034.
- [36] R.W. Farndale, D.J. Buttle, A.J. Barrett, Improved quantitation and discrimination of sulphated glycosaminoglycans by use of dimethylmethylene blue, Biochim. Biophys. Acta 883 (1986) 173–177, http://dx.doi.org/10.1016/0304-4165/86)90306-5.
- [37] C.F. Cesarone, C. Bolognesi, L. Santi, Improved microfluorometric DNA determination in biological material using 33258 Hoechst, Anal. Biochem. 100 (1979) 188–197, http://dx.doi.org/10.1016/0003-2697(79)90131-3.
- [38] G. Huszar, J. Maiocco, F. Naftolin, Monitoring of collagen and collagen fragments in chromatography of protein mixtures, Anal. Biochem. 105 (1980) 424–429, http://dx.doi.org/10.1016/0003-2697(80)90481-9.
- [39] R.M. Versteegen, R.P. Sijbesma, E.W. Meijer, Synthesis and characterization of segmented copoly (ether urea) s with uniform hard segments, Macromolecules 38 (2005) 3176–3184, http://dx.doi.org/10.1021/ma0478207.
- [40] J.E. Wagenseil, R.P. Mecham, New insights into elastic fiber assembly, Birth Defects Res. C Embryo Today 81 (2007) 229–240, http://dx.doi.org/10.1002/ bdrc.20111.
- [41] T. Shinoka, G. Matsumura, N. Hibino, Y. Naito, M. Watanabe, T. Konuma, et al., Midterm clinical result of tissue-engineered vascular autografts seeded with autologous bone marrow cells, J. Thorac. Cardiovasc Surg. 129 (2005) 1330–1338, http://dx.doi.org/10.1016/j.jtcvs.2004.12.047.
- [42] N. Hibino, E. McGillicuddy, G. Matsumura, Y. Ichihara, Y. Naito, C. Breuer, et al., Late-term results of tissue-engineered vascular grafts in humans, J. Thorac. Cardiovasc Surg. 139 (2010) 431–436, http://dx.doi.org/10.1016/ j.jtcvs.2009.09.057, 436.e1–2.
- [43] Y. Hong, J. Guan, K.L. Fujimoto, R. Hashizume, A.L. Pelinescu, W.R. Wagner, Tailoring the degradation kinetics of poly(ester carbonate urethane)urea thermoplastic elastomers for tissue engineering scaffolds, Biomaterials 31 (2010) 4249–4258, http://dx.doi.org/10.1016/j.biomaterials.2010.02.005.
- [44] D.E.P. Muylaert, G.C. Van Almen, H. Talacua, J.O. Fledderus, J. Kluin, S.I.S. Hendrikse, et al., Early in-situ cellularization of a supramolecular vascular graft is modified by synthetic stromal cell-derived factor-1α derived peptides, Biomaterials 76 (2015) 187–195, http://dx.doi.org/10.1016/j.biomaterials.2015.10.052.
- [45] P.Y.W. Dankers, M.C. Harmsen, L.A. Brouwer, M.J.A. van Luyn, E.W. Meijer, A modular and supramolecular approach to bioactive scaffolds for tissue engineering, Nat. Mater 4 (2005) 568–574, http://dx.doi.org/10.1038/nmat1418.
- [46] N. Hibino, G. Villalona, N. Pietris, D.R. Duncan, A. Schoffner, J.D. Roh, et al., Tissue-engineered vascular grafts form neovessels that arise from regeneration of the adjacent blood vessel, FASEB J. 25 (2011) 2731–2739, http:// dx.doi.org/10.1096/fj.11-182246.
- [47] N. Hibino, T. Yi, D.R. Duncan, A. Rathore, E. Dean, Y. Naito, et al., A critical role for macrophages in neovessel formation and the development of stenosis in tissue-engineered vascular grafts, FASEB J. 25 (2011) 4253–4263, http:// dx.doi.org/10.1096/fj.11-186585.
- [48] K. Garg, N a Pullen, C a Oskeritzian, J.J. Ryan, G.L. Bowlin, Macrophage functional polarization (M1/M2) in response to varying fiber and pore dimensions of electrospun scaffolds, Biomaterials 34 (2013) 4439–4451, http://dx.doi.org/10.1016/j.biomaterials.2013.02.065.
- [49] A.I.P.M. Smits, V. Ballotta, A. Driessen-Mol, C.V.C. Bouten, F.P.T. Baaijens, Shear flow affects selective monocyte recruitment into MCP-1-loaded scaffolds, J. Cell Mol. Med. 18 (2014) 2176–2188, http://dx.doi.org/10.1111/ icmm.12330.
- [50] I. Vesely, The role of elastin in aortic valve mechanics, J. Biomech. 31 (1997) 115–123, http://dx.doi.org/10.1016/S0021-9290(97)00122-X.
- [51] M. Votteler, D. a C. Berrio, A. Horke, L. Sabatier, D.P. Reinhardt, A. Nsair, et al., Elastogenesis at the onset of human cardiac valve development, Development 140 (2013) 2345–2353, http://dx.doi.org/10.1242/dev.093500.
- [52] G.J. Mahler, C.M. Frendl, Q. Cao, J.T. Butcher, Effects of shear stress pattern and magnitude on mesenchymal transformation and invasion of aortic valve endothelial cells, Biotechnol. Bioeng. 111 (2014) 2326–2337, http:// dx.doi.org/10.1002/bit.25291.

- [53] G.A. Skarja, J.L. Brash, P. Bishop, K.A. Woodhouse, Protein and platelet interactions with thermally denatured fibrinogen and cross-linked fibrin coated surfaces, Biomaterials 19 (1998) 2129–2138, http://dx.doi.org/10.1016/S0142-9612(98)00045-3.
- [54] J.Y. Hsieh, T.D. Smith, V.S. Meli, T.N. Tran, E.L. Botvinick, W.F. Liu, Differential regulation of macrophage inflammatory activation by fibrin and fibrinogen, Acta Biomater. (2016) 1–11, http://dx.doi.org/10.1016/j.actbio.2016.09.024.
- [55] J. Yoshioka, R.T. Lee, Vascularization as a potential enemy in valvular heart disease, Circulation 118 (2008) 1694–1696, http://dx.doi.org/10.1161/ CIRCULATIONAHA.108.809475.
- [56] E. Rabkin-Aikawa, M. Farber, M. Aikawa, F.J. Schoen, Dynamic and reversible changes of interstitial cell phenotype during remodeling of cardiac valves, J. Heart Valve Dis. 13 (2004) 841–847.
- [57] R. Khosravi, K.S. Miller, C a Best, Y.C. Shih, Y.-U. Lee, T. Yi, et al., Biomechanical diversity despite mechanobiological stability in tissue engineered vascular grafts two years post-implantation, Tissue Eng. Part A 21 (2015) 1529–1538, http://dx.doi.org/10.1089/ten.tea.2014.0524.
- [58] B. Weber, J. Scherman, M.Y. Emmert, J. Gruenenfelder, R. Verbeek, M. Bracher, et al., Injectable living marrow stromal cell-based autologous tissue engineered heart valves: first experiences with a one-step intervention in primates, Eur. Heart J. 32 (2011) 2830–2840, http://dx.doi.org/10.1093/eurhearti/ehr059.
- [59] S. Loerakker, G. Argento, C.W.J. Oomens, F.P.T. Baaijens, Effects of valve geometry and tissue anisotropy on the radial stretch and coaptation area of tissue-engineered heart valves, J. Biomech. 46 (2013) 1792–1800, http://dx.doi.org/10.1016/j.jbiomech.2013.05.015.